COTS Dust

by

Seth Edward-Austin Hollar

B.S. (Massachusetts Institute of Technology) 1996

A thesis submitted in partial satisfaction of the

requirements for the degree of

Master of Science
in

Engineering-Mechanical Engineering

in the

GRADUATE DIVISION

of the

UNIVERSITY OF CALIFORNIA, BERKELEY

Committee in charge:

Professor David M. Auslander, Chair
Professor Kristofer S. J. Pister
Professor David E. Culler
Professor Albert P. Pisano

Fall 2000

Table of Contents

List of Figures

Preface

The goal of this thesis is to provide information on cubic inch autonomous sensor devices otherwise known as Commercial-off-the-Shelf Dust (COTS Dust). COTS Dust is capable of sensing and responding to environmental changes and communicating to other devices. This thesis is the compilation of my experience and knowledge in the design of COTS Dust and can be considered a guide for those who wish to design similar systems. Ultimately, its my wish that material provided within contains enough information for those unfamiliar with this area of research to be able to design a working COTS Dust of their own in a relatively short time frame.

COTS Dust was originally designed for Smart Dust, an ongoing project whose goal is to make cubic millimeter autonomous sensor devices. In the introduction, I briefly describe how the design of Smart Dust necessitated the development of these larger prototypes, COTS Dust.

In section 2.0, I describe the subsystems requisite to the design of a fully autonomous system: power supplies, microprocessor choices, sensor suites, and communication possibilities. In so doing, I tried to point out the important design parameters to designing a reliable low power system.

In section 3.0, I describe all the devices I designed and built. To give the reader an idea of the functionality, each section describes a demonstration of the devices capabilities. Here, I point out the interesting design challenges that come about from making a fully operable system.

In section 5.0, I conjecture about future COTS Dust designs: marketplace trends and ongoing research. Lastly in the appendix, I include circuit board schematics and lists

of materials for most of the COTS Dust designs. Hopefully the technical information will serve as a starting platform for designing one's own COTS Dust.

1.0 Introduction

One way to realize what future technologies lie before us is to get a history lesson from the past. If you were alive five hundred years ago, would you have thought it was possible to talk to someone within seconds halfway around the world? Would you have even known the world was round? Civilization has been especially active in the last 150 years: the internal combustion engine, the atomic bomb, microelectronics, the human genome project. We take our knowledge for granted, but imagine being alive before the existence of hot water plumbing.

As much as our forefathers would find the present difficult to imagine, we, the present, find the future just as difficult to grasp. The farther out we project our future, the more difficult to predict. Nevertheless, by examining the current trends in technology, we gain a clearer vision of the future. Microelectronics offers one solid example of a consistent and commonly accepted trend to examine. Thirty years after its creation, Moore's law still rings true; the minimum process size continues to decrease. While microprocessor and memory companies try to squeeze progressively more transistors in a given area, the opposite can also hold true: for a given circuit, progressively less area is needed on the silicon wafer. Abstracting away from circuits, systems as a whole will also decrease in size while maintaining similar functionality as their predecessors. Further extending this cavalcade of projections, perhaps 25 years from now, today's Pentium III processor will fill less than one tenth of the area of the period at the end of this sentence.

Additionally, microelectro-mechanical systems (MEMS), a surrogate of the microelectronics industry, promises mechanical miniaturization. Together both MEMS and microelectronics provide the backbone of autonomous microsystems. One hundred years

from now, autonomous dust sized particles with capabilities to communicate and sense will number in the trillions, much like what Neil Stephenson created in his book, The Diamond Age [1]. Anything from monitoring weather patterns to tracking human movement might be possible with these incredibly functional, yet microscopic pieces of silicon dust. This miniaturization revolution is in part being realized by Professor Kris Pister's group at UC Berkeley through his project, Smart Dust [2, 3]. Smart Dust's ultimate goal is to create a fully autonomous system within a cubic millimeter volume.

1.1 Smart Dust Scenarios

What would one do with a "functional piece of sand?" With such a new concept the applications are plentiful. To give the reader a better understanding of useful applications for Smart Dust, I describe a few scenarios below.

1.1.1 Forest Fire Warning

A single device alone may have relatively small utility. For example, a single Smart Dust may be able to monitor the temperature at a single point, but it would not be able to monitor how the temperature changed over a region. The realization of Smart Dust's potential, however, lies in using large numbers. A million Smart Dusts distributed over a few acres of forest would not only be able to monitor the temperature at a million different points but also provide information in terms of traveling heat waves or moving cold fronts. Going a step further, processing can be performed on the temperature data to pinpoint the position and magnitude of a forest fire. Since the devices are autonomous they could offer continuous monitoring of the environment and alert the authorities the instant a forest fire is detected.

1.1.2 Enemy Troop Monitoring

Conventional ways to monitor enemy activity are either to use spy satellites or have manned hidden outposts. Both have drawbacks in regards to cost, risks to human life, and performance. Smart Dust, on the other hand, could offer a safer and cheaper alternative. With the ability to detect temperature, light, acceleration, and sound, Smart Dust could be scattered throughout a surveillance area. The dust particles would periodically record temperature, light, acceleration, and sound. Large vehicles like tanks would create vibrations in the ground that the silicon dust could detect. When queried by a laser interrogator system, the particles would upload their sensor data. While no one sensor would definitively detect a passing vehicle, the aggregate of sensors and dust particles would provide enough spatial sensor information, that when processed, would produce a robust vehicle detection scheme [4].

1.2 Smart Dust Capabilities

For this research, I assumed Smart Dust would have specific capabilities. Namely, Smart Dust would have four basic components:

1) **Power**. In order to monitor an environment for any length of time, the dust particle must have enough energy to survive anywhere from a few hours to months at a time.
2) **Computation**. Since the dust particle is expected to communicate and process sensor data, the dust particles must have computational requirements ranging anywhere from an 8 bit micro controller to a full blown 32 bit microprocessor.
3) **Sensors**. The interface between the environment and the dust particle is the sensor. The dust particles should have basic environmental sensors which may include temperature, pressure, humidity, light, sound, acceleration, magnetic fields.
4) **Communication**. Communication must be possible in standard outside environments. Dust particles must have the ability to communicate with one another at ranges from a few meters to kilometers.

With Smart Dust's low power requirements and large data gathering capabilities, a

number of questions have arisen in the areas of computing and communication.

1.2.1 Distributed Sensor Networks and Ad-hoc Networking

The scenarios described above are examples of distributed sensor networks, networks capable of sensing the environment and, in which, the individual devices can communicate with one another. Often times, Smart Dust will be scattered throughout an environment where the dusts' locations may not be known a priori. In order to pass information between devices, a network needs to be configured dynamically. Current research is investigating reconfigurable networks, also called ad-hoc networking.

1.2.2 High Level Interpretation of Spatial Sensor Data

Smart Dust offers the unique opportunity to gather large amounts of sensor data from multiple locations. The ensuing question is, "What can we discern from this wealth of information?"

For example, imagine a light sensor in a room in a house. The light sensor records light continuously, and if we examine how light changes over time, we may be able to draw some conclusions. During the times of high light readings, can we safely conclude that the light switch in the room was turned on? Can we assume that someone is in the room when the light is on? Can we assume no one is in the room when the light is off? Obviously, some of our conclusions will be in error, but by collecting more information, the conclusions may come closer to reality.

Within this example, now add a sound sensor in the room. If occurrences of high light intensity and loud noises are concurrent in the room, can we assume there is someone in the room? Perhaps more so than in the original scenario. Going one step further, we

can include a number of sensors in every room of the house. The sensor set may include light, temperature, and sound. Suppose now, only one room in the house is reading high levels of light and sound, and that room's temperature is a few degrees higher than any other room in the house. We are even more certain that someone is in that room.

The example above illustrates how multiple nodes and sensor data can aid in gaining a high level understanding of the activity in a given area, otherwise known as data fusion. While a single raw sensor may not provide a good understanding of high level activity, the inclusion of spatial data and multiple sensors can lead to a fairly accurate high level conclusion.

1.2.3 Distributed Processing

In order to interpret spatial sensor data, the data must to be collected and processed in an organized fashion. One method is to gather all the data and transfer it out of the network where the data can be analyzed. However, a connection to the network may be only accessible temporally or may have limited throughput, making it difficult to continuously monitor and analyze large amounts of sensor data. The other possibility lies in doing the analysis of the data within the network itself. As opposed to doing the processing on a single computer, the processing could be distributed among all the dust particles, each of which acts as a minicomputer. After the completion of the analysis, the results could then be transferred out of the network.

Distributed processing is a research area in itself. Depending on the communication constraints of the system, algorithms must be developed that would allow individual dust motes to share and process data efficiently.

1.2.4 COTS Dust

Because the length of time to develop a complete Smart Dust system was on the order of years, there needed to be an alternative means to test basic behavior in a timely manner. To this end, COTS Dust was created. The quickly-developed prototypes were built using commercial-off-the-shelf components (COTS). COTS Dust had all the basic functionality of Smart Dust, but the devices were built in a tenth of the time. Instead of being a cubic millimeter in size, these devices were a cubic inch in size. COTS Dust could serve as a platform to run a variety of algorithms to test various behaviors that Smart Dust would exhibit.

In addition to providing a method to test basic Smart Dust functionality, COTS Dust could also be used in other ways. Namely, COTS Dust could be used as a data logger, warehouse monitor, and any other application where environmental monitoring can be performed with palm size devices. For example, conventional data loggers which record weather information often require a physical connection to download the data. COTS Dust can be made to be $1/20^{th}$ the size and yet be able to send data remotely to the end user [5].

The novel aspect of COTS Dust is that it takes advantage of the fact that individual components in microelectronics are shrinking in size and power and increasing in functionality. Products that were cumbersome and unwieldy ten years ago can be designed to fit in the palm of one's hand today.

2.0 COTS Dust Architecture

COTS Dust was designed with simplicity in mind; the goal being functional generic devices that would provide a fast prototyping tool to test the behavior of Smart Dust. In order to emulate their behavior, COTS Dust assumed the four basic subsystems found on page 3.

I designed and built several COTS Dust devices. All the COTS motes, as I referred to them, followed a similar architecture but differed in sensor medley and communication type. A diagram of the basic architecture can be found in Fig. 1 on page 8. An Atmel AVR microcontroller served as the brain, while depending on the flavor of the device, either optical or RF communication was used. Most COTS devices were powered by a 3V lithium battery. Lastly, each device had its own sensor suite chosen from the following list: magnetometers, accelerometers, light sensor, temperature sensor, pressure sensor, and humidity sensor.

The following sections describe the subsystems in more detail.

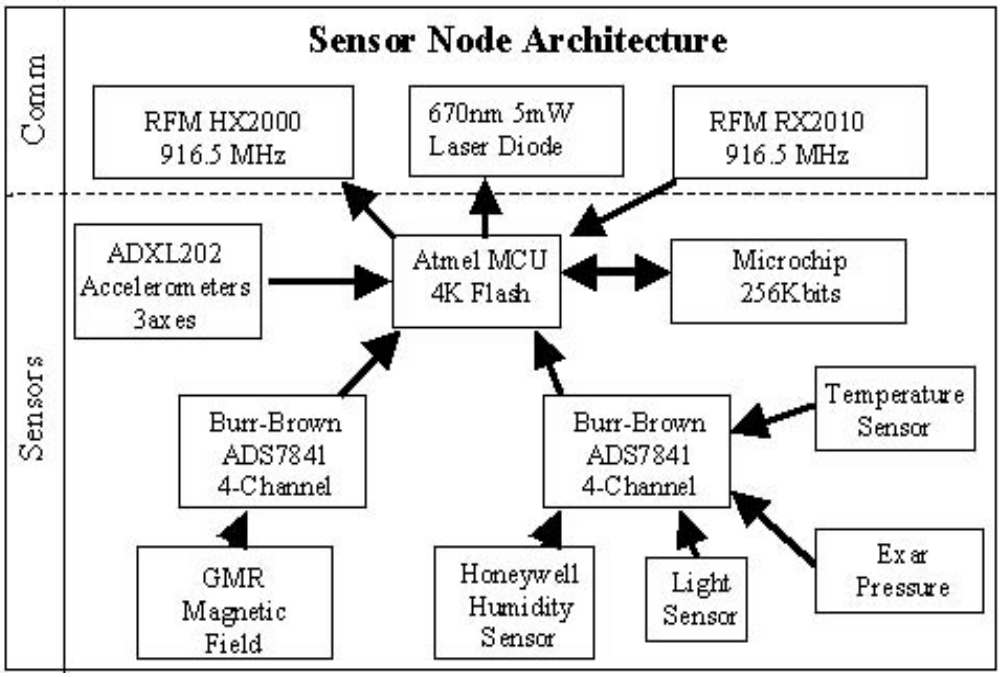

Fig. 1. Architecture for COTS Dust.

2.1 Power

One of the tightest constraints on the circuit design was the operating voltage. Assuming the device would be operated using batteries, careful attention was paid to the available operating voltage. Because the RF chip sets in the design required a very narrow operating range centered at 3 Volts, I focused on 3V portable power sources. Table 1 on page 9 compares three types of batteries. Lithium batteries not only offered the greatest energy density but also operated at the desired 3 Volts. Even though Lithium batteries had the highest energy density, they did not, however, have the highest current capacity. The Nickel-metal hybrid batteries could output over 260 times more current per unit mass.

Aside from the fact that adding a voltage regulator would complicate the design of the COTS Dust, voltage regulators required additional power to run, added noise to the

system, and increased the parts count for the COTS Dust design. Therefore, I focused my efforts on designing the system and battery to operate at the same operating voltage.

To operate for long periods of time, the COTS Dust was designed to enter sleep mode in order to save power. Virtually all microprocessors on the market can go into low power modes. However, I found that very few processors consumed less than 1 μW while sleeping. It was important to have a very low sleep current because long sleep periods could drain a significant amount of the battery.

To avoid this complication, some of the COTS devices made use of the Dallas Semiconductor DS1306E. The DS1306E was a real time clock with alarm and had an average power drain of 1μW. The DS1306E's alarm could be programmed to turn off power to the processor, guaranteeing COTS Dust an overall sleep power dissipation of 1 μW.

Table 1: Battery Types

Battery Type	Voltage	Energy Density	Max Current
Alkaline AA P107-ND	1.5 V	90 mWatt-hrs/gram	130mA @ 24 grams
Nickel-Metal Hybrid (recharchable) P014-ND	1.2 V	55 mWatt-hrs/gram	>2600mA @ 26 grams
Lithium	3.0 V	285 mWatt-hrs/gram	10mA@10.5 grams

2.2 Computation

To act as the brain of the COTS Dust, a suitable computation subsystem had to be chosen. Both microprocessors and FPGAs offered off-the-shelf solutions and adequate computation power. In addition to consuming more power, the FPGAs were not compatible with traditional programming methodologies (i.e. no C compiler). Taking into consideration the modest computational needs of the system, I chose 8 bit microcontrollers

because they realized the lowest power consumption and contained internal program memory. Additionally, most 8 bit MCUs contained instruction sets and software tools that were easy to learn.

Table 2: Comparison of Microprocessors

	Atmel AVR AT90LS8535	Microchip PIC16F877 (preliminary)	MC68H(R)C 908JL3	Atmel AT91M404000 16/32 bit Strong Thumb
Flash Memory	4K	8Kx14	4K	external memory
Endurance	1k	1k	10k	N/A
MIPS/mA	1.25 (min)	1.66 (preliminary)	0.1 (typical)	0.6 MIPS/mA (1.35 mA static current)
A/D channels	8 (10 bit)	8 (10 bit)	12 (8 bit)	0
In-application programming (IAP)	no	yes	yes	yes
Operating voltage	2.7-5.5V	2.0 - 5.5V	2.7-3.3V	2.7V-3.6V
I/O pins	35	40	23	100

The important features specific to picking a microprocessor were 1) power, 2) memory size, 3) fast reprogrammability, 4) A/D channels, and 5) a 3 volt operating supply. Table 2 on page 10 compares the most suitable microprocessors for COTS Dust on the market. Though not an 8 bit processor, the Strong Thumb processor was included both because of its commercial popularity and low power consumption. At the time the Atmel AT90LS8535 offered the best performance even though newer designs like the Microchip PIC16F877 offered lower power consumption and greater functionality.

2.2.1 Static vs. Dynamic Current

Since clock frequency was proportional to power consumption, MCUs can be run at low frequencies for low power operation. However, the relationship is not entirely linear. If the frequency of the MCU is low enough, power consumption is determined by the DC static current, not the frequency of the MCU. For example, the Atmel AT90LS8535 had a static current of 1.28 mA and a dynamic current of 0.81 mA/MIPS whereas the Microchip 16F87x had a static current of 15 μA and a dynamic current of 0.6 mA/MIPS.

In terms of power consumption, it made no sense to run the Atmel processor any less than 100 KHz because the total current consumption was within 10% of the static current. Whereas for the Microchip MCU at 100 KHz, power could be reduced by a factor of 5 by lowering the clock frequency even further. For ultra-low power processors, one would want to use a low frequency clock and a processor with low static current.

2.2.2 Strong Thumb

Strong Thumb is a 32 bit processor core which is licensed by ARM to international electronics companies [6]. The unique distinction between the Strong Arm and Strong Thumb is that the Strong Thumb also contains a full 16 bit instruction set. Even though the microprocessor is 32 bits, a 16 bit instruction set reduces the size of each instruction by half effectively doubling the amount of memory space. Its low power design made it an especially attractive competitor to the 8 bit MCUs if nothing else but for its floating point computation capabilities.

Because the Strong Thumb is strictly a processor core, I could not compare its features directly with that of discrete MCUs. Instead, I chose Atmel's AT91M404000 16/32 bit Strong Thumb as a basis for comparison. Though it has no ADCs and its power con-

sumption is three times that of the competing 8 bit MCU, the Strong Thumb is a possibility for future COTS devices demanding more computational power. Furthermore, Strong Arm processors have a well established set of debug tools and C compilers making them particularly attractive to software designers.

2.3 Sensors

Sensors provided the raw data the COTS Dust needed to gain a high level understanding of the environment. With that in mind, I chose sensors which extracted telling information from their surrounding. The sensors themselves could be classified into two groups: 1) weather monitors, and 2) motion detectors. The following sections elaborate further on the distinction between the two groups. Table 3 on page 12 summarizes the sensors used in COTS Dust.

Table 3: Sensor Specifications

	Current consumption	Voltage range	Min range/ Max range	Accuracy	Temperature dependence	Product
Magnetometer	650µA	2.7-5.25V	-/+0.5 Gauss	2 mGauss	1.4mG / °C	AA002-02 NVE
Accelerometer	600µA	3-5.25V	-/+2g	25 mg	negligible	ADXL202 Analog Devices
Light sensor	200µA	2.7-5.5V	0 mW/m^2 / 26 mW/m^2	6 mW/m^2	negligible	H53371 Edmund Scientific Silicon Detector
Temperature sensor	600µA	2.7-5.5V	-20°C/100°C	0.25°C	not applicable	AD7418 Analog Devices
Pressure sensor	650µA	2.7-5.5V	0.6 PSI gauge range @ 14.4 PSI absolute	2.4 mPSI	10 mPSI/°C	SM5310 SMI

Table 3: Sensor Specifications

	Current consumption	Voltage range	Min range/ Max range	Accuracy	Temperature dependence	Product
Humidity sensor	200μA @5V	4-9V	0-100% relative humidity	+/-2% RH	negligible	HIH-3605 Hy-Cal

2.3.1 Magnetometer (2/3 Axis)

Magnetometers are sensors that measure magnetic fields. They can measure the 60 Hz fluctuations from power lines or the Earth's naturally occurring magnetic field. The magnetometers used in COTS Dust were magneto-resistive elements configured in an H-Bridge.

To implement magnetometers into COTS Dust, I designed the circuit shown in Fig. 2 on page 14. The magnetometers were followed by a two-stage amplifier design with a total voltage gain of 284. The analog signal was then digitized by a 10 bit ADC. Because a Lithium battery's voltage dropped from 3.3V to 2.7V over its lifetime, the circuit was designed to withstand power supply fluctuations. The output of the circuit was described by Equation 1:

$$\frac{V_{out}}{V_{cc}} = G_2\left(\frac{\Delta R}{2R}G_1 + \frac{1}{2} - \frac{R_{variable}}{R_{totalpot}}\right). \quad (1)$$

If V_{cc} fluctuated, so did V_{out}, but since the output was sampled by an A/D converter whose reference point was V_{cc}, the digital value was left unchanged, at least to first order.

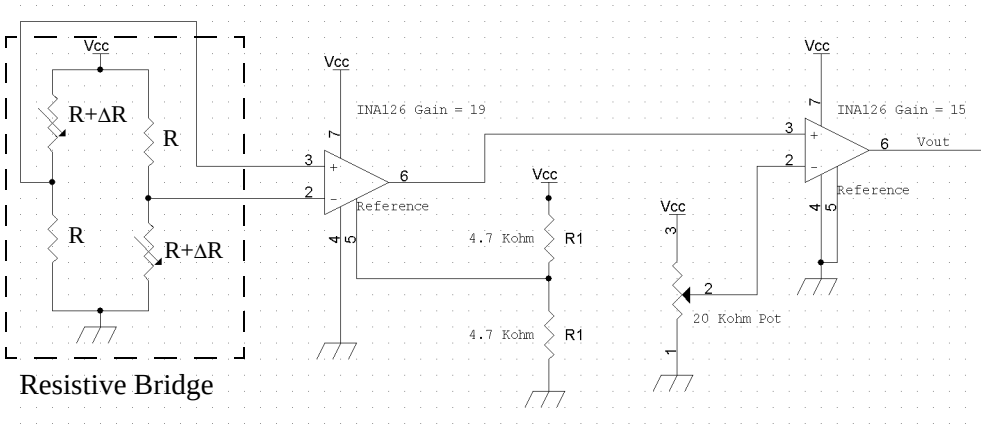

Fig. 2. Circuit diagram of magnetometers.

The magnetometers were designed such that they can detect the Earth's magnetic field. Since each magnetometer could measure the magnetic intensity along a single axis only, three mutually perpendicular magnetometers were needed to extract the full vector of the Earth's magnetic field. By rotating the COTS Dust, the Earth vector rotated in the frame of the device, allowing the device to detect rotational movement. Going one step further, since the Earth's magnetic field changes both in intensity and direction over the globe, the device could theoretically be able to extract the geographic latitude.

Though the magnetometers were accurate to 2 mGauss, they were vulnerable to large magnetic fields. Fields in excess of 15 Gauss permanently changed the sensitivity of the sensors, requiring a recalibration.

2.3.2 Accelerometers (2/3 Axis)

The Analog Devices ADXL202 was a MEMS type accelerometer which used capacitive sensing to measure distance between a reference mass and a proof mass. The output of the ADXL 202 was a pulse-width modulated signal whose duty cycle was pro-

portional to acceleration. The Atmel microprocessor measured the period of the pulses to determine the correct acceleration measurement.

The word, accelerometer, is a bit of a misnomer because force is the unit really being measured. The most striking example is that accelerometers can measure the magnitude and direction of gravity. Like the magnetometers, three mutually perpendicular accelerometers were needed to fully resolve the magnitude and direction of any force. In a static situation (i.e. when the sensor was immobile), the gravity vector was the only force acting on the accelerometers. Partial orientation information could be obtained based on the gravity vector's relationship to the frame of the sensor, much the same way the Earth's magnetic field yielded orientation information. The gravity vector in conjunction with the magnetometers could provide exact orientation information. Of course, under actual acceleration, the gravity vector could not be extracted.

The accelerometers played a key role in developing a derivative of the COTS Dust devices, the Acceleration Sensing Glove [7] (see Fig. 3 on page 16). Because gravity can provide orientation information, static hand gestures could be interpreted into computer symbols by placing accelerometers on the fingertips of a hand.

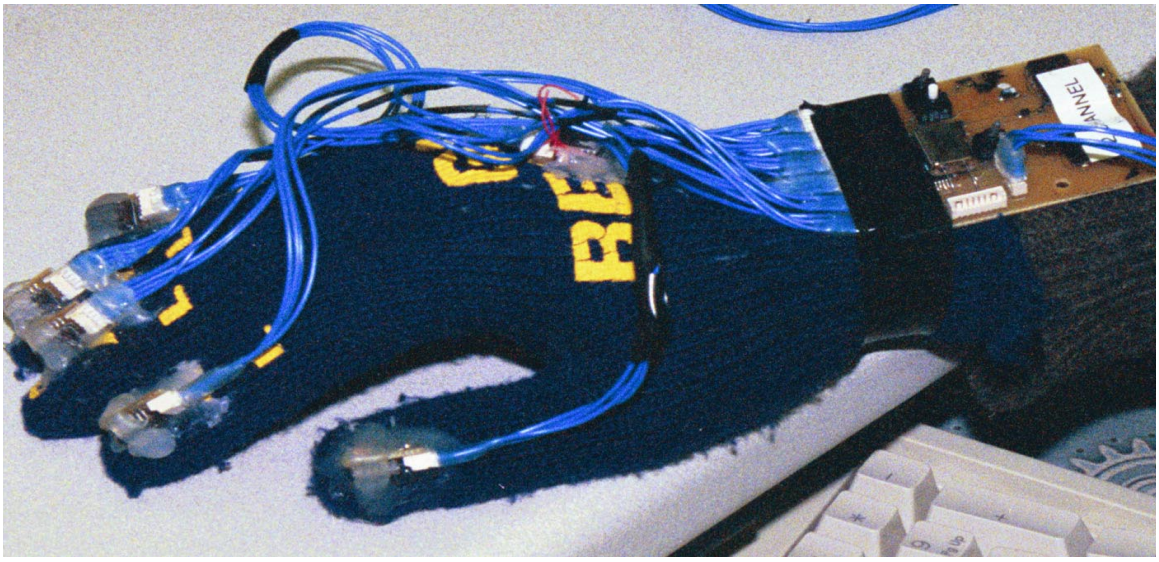

3. Acceleration Sensing Glove (virtual keyboard). Accelerometers can be used to translate hand gestures int
puter interpreted signals.

2.3.3 Light Sensor

The light sensor was designed with a photodiode and transresistance amplifier (Fig. 4 on page 17). Depending on the resistor chosen, the light sensor's sensitivity could be adjusted for either sunlight or room light. The output of the amplifier was then digitized by a 10 bit ADC.

The bandwidth of the light sensor on the Laser Mote (see "Laser Mote" on page 49) was over 1KHz. As described later in "Photodiode Downlink" on page 53, the light sensor was a communications receiver where modulated light was used to send binary data.

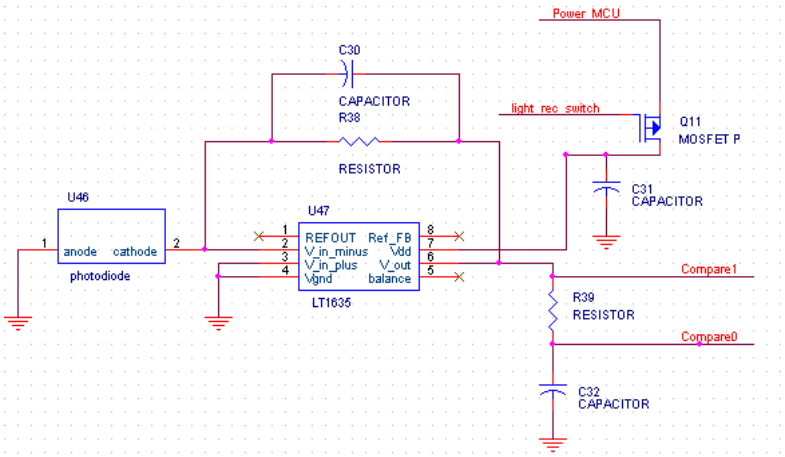

Fig. 4. Circuit diagram of light sensor.

2.3.4 Temperature Sensor

Most COTS Dust designs incorporated the AD7418. The output of the temperature sensor used the I^2C protocol to transmit digital information to the microcontroller. With a full range from -20°C/100°C the AD7418 required no calibration and had an accuracy down to 0.25°C.

2.3.5 Pressure Sensor

The SM5310 was an uncompensated silicon sensor chip whose resistance changed as a function of pressure. The device came in a resistive H bridge package, and its output was amplified by a two-stage amplifier design similar to that of the magnetometer (Fig. 5 on page 18). The output was then digitized by a 10 bit ADC.

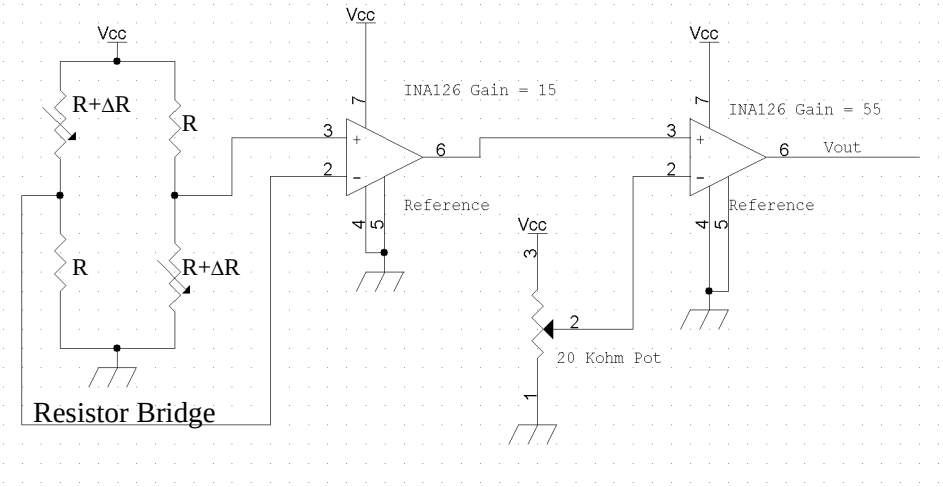

Fig. 5. Circuit diagram of pressure sensor.

In addition to providing weather information, the pressure sensor could be used as a motion sensor. Since pressure decreases at higher altitudes, the sensor could act as an altimeter. Referring to Table 3 on page 12, the accuracy of the pressure sensor circuit was 2.4 mPSI, and according to Table 4 on page 19, the change in pressure as a function of altitude is approximately 0.5 mPSI/foot, suggesting the sensor could detect altitude changes of 5 feet or greater.

While the circuit could detect small gradations in altitude, it had a strong dependence on temperature, namely 10 mPSI/°C. In other words, in order for the pressure sensor to maintain its sensitivity of 2.4 mPSI, the temperature would have to be accurately measured to within 0.25 C for calibration purposes. Further work needs to be conducted to verify the true accuracy of the pressure sensor.

Table 4: Pressure vs. Altitude - adapted from [8],

Altitude Above Sea Level (feet)	Equivalent Pressure (PSI)	Approximate Slope mPSI/ foot
0	14.7	-0.52
3000	13.17	-0.48
6000	11.78	-0.44
8000	10.91	-0.43

2.3.6 Humidity Sensor

The capacitive humidity sensor was a fully integrated circuit whose output voltage was linearly proportional to relative humidity. Its low power design (200μA) and ease of integration made it an almost ideal candidate to the suite of sensors used for COTS Dust. However, its specified voltage range of 3.9V-9V made it difficult to integrate with the Lithium batteries. Qualitatively, the humidity sensors operated at 3 Volts, but quantitative analysis was not performed to determine the degradation in accuracy.

2.4 Communication

One of the basic assumptions of both COTS Dust and Smart Dust was that motes would communicate with others wirelessly. The intention in Smart Dust was to use optical communication. For COTS Dust, however, I explored alternative means of communication. In as far as wireless communication goes, I imagined three possibilities: 1) Acoustic 2) RF and 3) Optical. The emphasis, again, was placed on low power operation and ease of design and implementation. The three possible communication scenarios are

outlined below.

2.4.1 Acoustic Communication

Acoustic communication was initially investigated as a possible candidate for COTS communication. However, three factors limit the capabilities of small, low power transducers. First, the size of the transducer limits the total acoustic output power. Second, the surrounding background noise limits both the minimum strength of the transmitted signal and total data throughput. Lastly, the atmosphere attenuates signal power over large distances. In this section, I discuss each of these limitations and describe the basic equations used to estimate power consumption and data rate in acoustic communications

Signal strength depends on the size and vibrational amplitude of the transducer. Most transducers create sound by inducing a drum to vibrate. The drum in turn vibrates the air surrounding it, ultimately producing sound. Raleigh's first integral [9] describes the interaction of plane structures with semi-infinite fluid volumes and provides a first approximation to estimate the strength of a transducer.

$$p(r,t) = \frac{i\omega\rho_o}{2\pi} e^{i\omega t} \int_S \frac{V_n(r_s) e^{-ikR}}{R} dS . \quad (2)$$

where p(r,t) is the pressure,
ω is the circular frequency,
ρ is the density of air,
R is the distance from the surface element,
and $V_n(r_s)$ is surface normal velocity.

For a transducer whose size is much smaller than the wavelength, Equation 2 can be simplified to yield the following relationship:

$$\langle I \rangle \propto \left(\frac{AS\omega^2}{R} \right)^2 . \quad (3)$$

where <I> is the timed average acoustic intensity,
A is the amplitude of vibration of the transducer, and
S is the surface area of vibration.

As the size of the transducer is miniaturized, both A and S become smaller limiting the total output power of the device. As geometry suggests, the intensity drops off as the square inverse of thee distance. These effects are clearly exemplified in Smart Dust. Since the size of Smart Dust is no larger than a cubic millimeter, the dimensions of the transducer are also limited to a cubic millimeter. For example, if the drum area is 1 mm^2, the peak-to-peak vibrational amplitude is 0.3 mm, and the bandwidth is 10 kHz, at 10 meters away, the transducer maintains a sound pressure level (SPL) of 50.5 dB. At 5% efficiency, the transducer consumes 10 milliwatts. To give the reader an idea of SPL, Table 5 describes the various SPL levels for common sounds.

Table 5: Typical Sounds and their SPL

Sound	SPL
passenger compartment of car on freeway	70
average conversation (3 feet)	60
average suburban home (at night)	50
quiet auditorium	40
quiet whisper	30
very quiet recording studio	20
threshold of hearing	0

Data rate is not linked directly to the SPL of the transducer, but instead to the Signal-to-Noise ratio (SNR) of the signal. Shannon's Law specifies the maximum theoretical data rate of a system based on its bandwidth and SNR:

$$C = BW\log_2(1 + SNR) . \quad (4)$$

where C is the data rate and BW is the bandwidth.

As SNR increases, the maximum theoretical data rate also increases. Since SPL is a measure of power in acoustics, the SNR is easily determined by the SPL of the signal and the background noise. Referring to the previous example, the transducer maintains a signal SPL of 50.5 dB. If the background noise is 45 dB SPL, then the maximum theoretical data rate is 22 kbps. In terms of energy, it costs 120 nJ to send each bit. Of course, this represents the maximum possible data rate. In real systems, data rates sometimes fall well below this limit.

Lastly, signal bandwidth is limited by the atmospheric absorption of sound waves at high frequencies. While Equation 3 suggests that higher frequencies enable the transducer to output more power, atmospheric attenuation also increases with increasing frequency. For typical environmental conditions (30% RH at 20°C), a 10 KHz sound wave is attenuated by 20 dB after traveling 100 meters whereas a 1 KHz wave is attenuated by only 0.5 dB [10].

Acoustic receivers, however, consume relatively little power. For example, a Knowles Electronics' hearing aid microphone has a bandwidth up to 10 kHz, a noise floor of 27 SPL, and a power dissipation of 24 μW. As one possible use, acoustic receivers can act as low power monitoring units. Motes in listening mode can wake up when they are signaled by neighboring devices.

The above analysis describes the theoretical limitations of acoustic communications. I did not pursue acoustic communications for COTS Dust because small form factor acoustic communication systems were difficult to find in the commercial market place. In addition, the theoretical analysis for acoustic communication suggests that transmitter

power dissipation was comparable to Bluetooth, an RF standard described later in the thesis (see page 24). For Smart Dust, the total output power of the transducer was limited by its small size. Furthermore, the background noise severely limits the environment where acoustic communication can be effective. While it may be possible to communicate in a quiet forest, background noise levels wash out signal levels in indoor areas.

As opposed to acoustics, RF and optical communications offer practical COTS Dust systems and associated small scale solutions. These systems are described in the following sections.

2.4.2 RF Communication

RF communication is based on electromagnetic waves with frequencies ranging from tens of kHz to hundreds of GHz. Of the many factors to include in RF communications, perhaps one of the most important in cubic millimeter devices is antenna size. To optimize transmission and reception, an antenna should be at least $\lambda/4$, where λ is the wavelength of the carrier frequency. Assuming a quarter wavelength to be 1 mm, the length of a Smart Dust particle, the RF carrier frequency would have to be 75 GHz, which is slightly out of the range of modern low power RF electronics. One possible solution to this dilemma is to include conductive tails on the devices to extend the length of the antenna. Tails would act as effective antennas but be light enough so as not to affect the small form factor of Smart Dust. While possible, RF communication was not pursued in Smart Dust. However, its ease of use and integrability made it an ideal testing platform for COTS Dust.

Additionally, RF is well established in the commercial marketplace. In the area of MEMS, ongoing research is investigating the use of steered agile beams [11] but no ready

made products are currently available.

2.4.2.1 Bluetooth

Bluetooth is an emerging standard that provides for the specification of small-form factor, low-cost, short range radio links [12]. The Bluetooth standard provides specifications for the radio link, baseband link, and the link manager protocol. The radio link specifies factors like the RF power, frequency spectrum, and modulation scheme. The baseband specifies the architecture of the message packets, including training sequences and CRC's. The manager protocol specifies how devices communicate with one another, including determining master and slave, controlling data rate, and forming networks. At present, few Bluetooth compliant devices or fully integrated chip sets on the market. Nonetheless, considering the influence Bluetooth may have on future COTS Dust, I would like to summarize its capabilities below.

In the radio link, the Bluetooth standard can support data rates up to 1 Mbps, specifying 79 channels between 2.402 and 2.480 GHz worldwide. Designed to function smoothly in noisy environments, Bluetooth devices can perform up to 1600 hops/second. Three classes of transmitting powers exist for the bluetooth standard depending on the range of communication: Class 1 20dBm (100 mW), Class 2 4 dBm (2.5 mW), and Class 3 0 dBm (1 mW). Bluetooth can also minimize power consumption by minimizing the transmission power based on the strength of the received signal.

For the link management protocol, multiple Bluetooth devices can form small groups called piconets in which there is one master and multiple slaves. Overlapping piconets are called scatternets. Each master device is capable of establishing comm links with multiple slaves simultaneously. In addition to providing 16 bit cyclic redundancy

checking, the Bluetooth standard also employs error correction and a repeat request scheme to account for lost transmissions.

While the Bluetooth standard promises to provide an easy way for devices to communicate with one another, there are as yet few fully compliant Bluetooth chipsets on the market. To further frustrate the problem, the devices available on the market place often require a 100 mW. To compare Bluetooth devices with those of RF Monolithics (“RF Monolithics” on page 25), I chose the Philstar PH2401 transceiver chip which satisfies the radio specification (see Table 6 on page 25). It should be noted that the PH2401 supported the radio specification only and did not include the baseband and link management specifications. More information on Bluetooth can be found in [13].

Table 6: RF Transceiver Comparisons

	HX2000 Transmitter	RX2010 Receiver	Blue Tooth Compliant Philstar PH2401
Modulation Type	OOK	OOK	GFSK
Carrier Frequency	916.5 MHz	916.5 MHz	79 Channels (2.402 to 2.480 GHz)
Operating Voltage	3 V	3 V	1.8V
Current Consumption	4.5 mA	2.5 mA	<20mA
Throughput	>10kb/s	10kb/s	1 Mbit/s
Receiver Sensitivity	N/A	-74 dBm	-84 dBm
Transmitter Power	0dBm	N/A	+2dBm

2.4.2.2 RF Monolithics

RF Monolithics is a company that specializes in the design and manufacture of low power RF systems [14]. One of their products, the TR1000, is a hybrid transceiver, designed for short-range wireless data applications. The TR1000 employs RFM’s ampli-

fier-sequenced hybrid (ASH) architecture and at the time, was one of the few complete RF transceiver multi-chip modules available on the market. The device consumes an average of 18 mWatts of power with bit rates up to 115 kbps with amplitude shift keying (ASK) and 19.2 kbps with on-off keying (OOK).

Other transceiver chips I investigated required numerous external capacitors and inductors, potentially compromising the simplicity of the COTS Dust design. RFM's hybrid transceiver required at most a dozen external components.

The transceiver operated with a carrier frequency of 916.5 MHz, and COTS Dust operated the transceiver using OOK modulation. The TR1000 supported the radio link only and did not specify a baseband or link layer like that of Bluetooth. The baseband layer was implemented through the Atmel MCU.

The packet protocol chosen for most COTS Dust devices is displayed in the diagram below (Fig. 7 on page 27). To maximize SNR in the receiver, RF Monolithics recommends DC balancing the RF signal. DC balancing means sending a roughly equal number of high bits as low bits. Manchester encoding was implemented on top of the raw data bit stream. Manchester's straightforward nature and inherently DC balanced signal made it easy to implement. Manchester encoding scheme is shown in Fig. 6 on page 27. As seen, a "1" representation is a high bit followed by a low bit, and a "0" representation is a low bit followed by a high bit.

A training sequence of alternating high and low bits was used to equalize the DC balance of the receiver. Afterwards a flag byte was used to signal the beginning of the packet protocol. The flag byte I chose was somewhat arbitrary. While a normal flag byte is usually 01111110 I chose 01110110 so that it would differentiate itself more from the

training sequence. The first byte after the flag byte specified the total data bytes in the packet. The following bytes were then the data bytes. Lastly, a 16 bit CRC (cyclic-redundancy check) indicated if the integrity of the data packet had been compromised.

With the above packet protocol data packets could contain anywhere from 1 to 255 bytes with insured data integrity. Instead of being optimized for compactness, the protocol above was designed with ease of use in mind. For example, block encoding provides tighter data compression with the cost of additional processing.

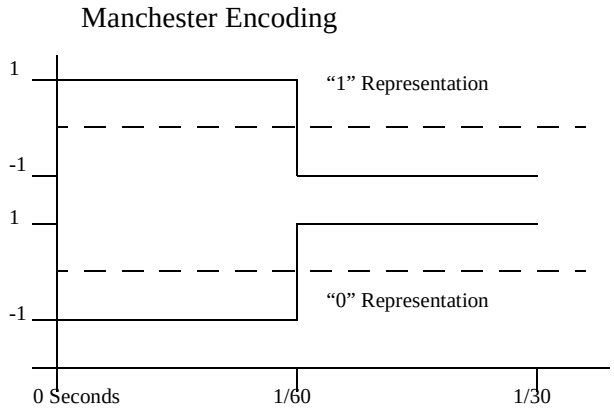

Fig. 6. Manchester Encoding with 1/60s pulse widths.
One and zero representation.

Training Sequence	Flag Byte	Number of Bytes	Data Bytes	2 Byte CRC

Fig. 7. Communication packet sequence used in COTS dust devices.

2.4.3 Optical Communication

In optical laser communication, a transmitting device uses a laser beam to send information. An optical receiver, either in the form of a photodiode or CCD array receives

the signal and decodes the data. Optical communication can be classified into two types 1) passive communication and 2) active communication. In active optical communication, the transmitting device generates its own laser signal whereas in passive communication, the laser signal is generated through a secondary source.

2.4.3.1 Passive Laser Communication

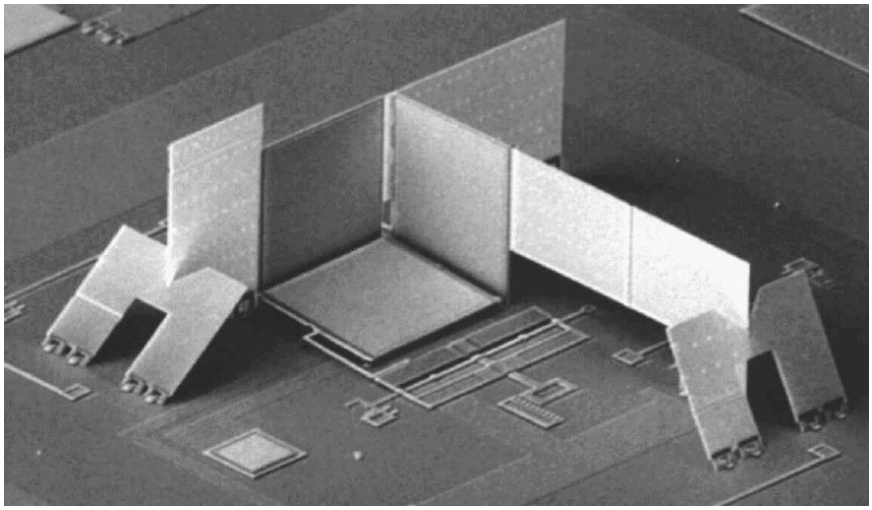

Fig. 8. SEM of Corner-Cube-Reflector. Scanning electron microscopy photo of corner cube reflector from MUMPS process. Courtesy of Victor Hsu.

The first versions of Smart Dust employ passive optical communication through the use of MEMS corner-cube-reflectors (CCR) [15, 16]. A CCR is a device composed of three mutually orthogonal mirrors which reflect light directly back to the laser source (see Fig. 8 on page 28). By offsetting one of the mirrors a few degrees from the normal, the CCR can scatter the light such that very little signal comes back to the source. Fig. 9 on page 29 demonstrates the concept in the 2-D case. By modulating the mirror, which modulates the light seen at the source, the CCR mote can communicate without generating a light source of its own.

The appealing quality of the CCR is that it is extremely low power, not having to

generate a laser source of its own. The cost of transmission is limited to the energy required to deflect one of the mirrors, which in the case of the MEMS CCRs used in COTS Dust amounts to 100 pJ/bit. The asymmetric nature of the communication system, though, requires one device to generate the laser while the other device has an integrated CCR For more information see “Corner Cube Reflector Mote (CCR Mote)” on page 52.

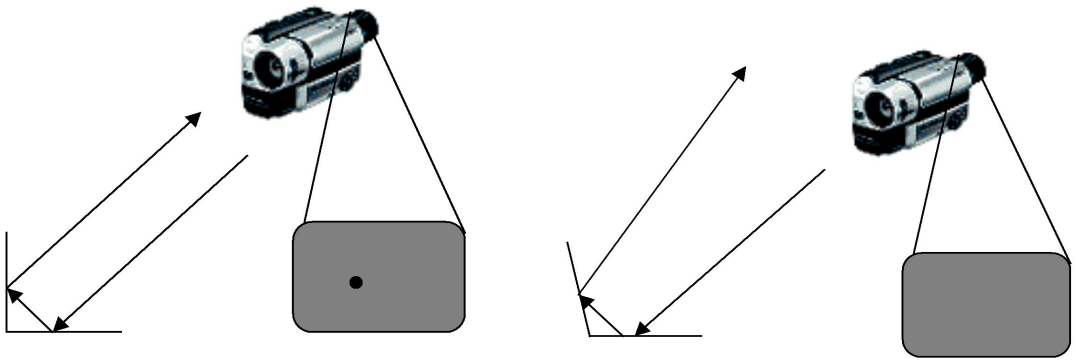

Fig. 9. Corner-Cube-Reflector Example. Demonstration of operation of corner cube reflector. In left picture, light reflects back to source when all mirrors are mutually perpendicular. In right picture, light scatters, when one mirror is a few degrees from the perpendicular.

2.4.3.2 Active Laser Communication

In active laser communication, the laser is on board the transmitting device. In COTS Dust, the laser was a laser module used in laser pointers. To give the reader an idea about the characteristics of a laser module, I have included Table 7 on page 30 outlining the RSa670-5 from Power Spectrum.

Table 7: Laser Module RSa670-5 from Power Spectrum

Full Width Divergence	1.2 millirad
Optical Power	3.0-3.3 mWatts
Wavelength	670 nm
Power	50mA @ 3V

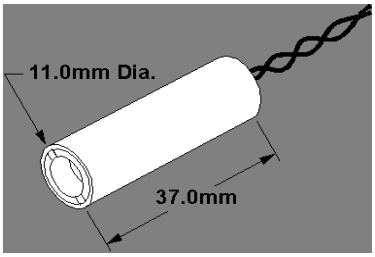

Fig. 10. Laser Module Diagram. Typical laser module used in COTS Dust

Active laser communication involves pointing the laser in the direction of an optical receiver and modulating the laser to transmit data. With divergence angles in the milliradians, lasers maintain a high optical intensity, enabling transmission over long distances. On COTS Dust devices, laser communication was established at distances up to 21.4 km (see “Laser Mote” on page 49).

Unlike most RF communication systems, however, active laser communication involves a spatial acquisition step. The laser beam of the transmitting device needs to be pointed in the direction of the optical receiver. Depending on the acceptance angle of the optical receiver, the receiver may also need to be aligned to the laser. Figure 11 shows a simple 2-D diagram of a laser transmitter coaligned with an optical receiver.

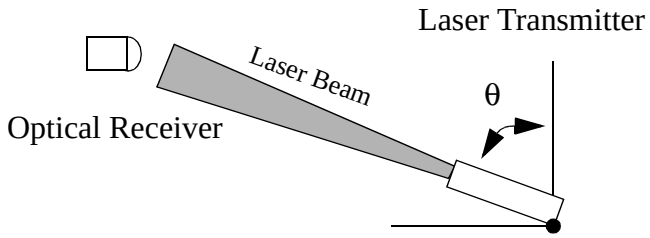

Fig. 11. 2-D Laser Comm. Here the spatial acquisition step involves setting θ such that the optical receiver falls within the laser beams illuminated area.

As can be seen, θ must be chosen such that the receiver falls within the beams illuminated area. When the locations of the receiver and transmitter are known a priori, the spatial acquisition step involves simple mathematics to choose θ such that communication can be established. However, when the locations are not known, a search algorithm needs to be executed to discover their relative locations.

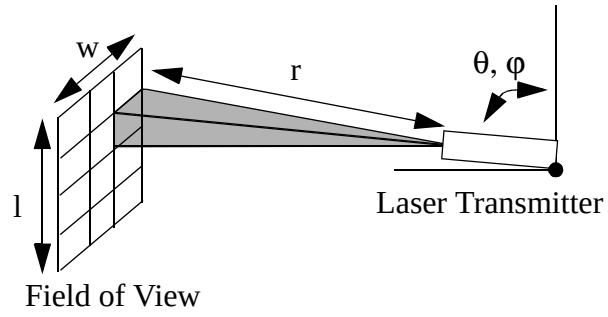

Fig. 12. 3-D Spatial Search. The laser must search the entire field of view to find an optical receiver. The number of search locations depends on the divergence of the laser beam and the size of the field of view.

When searching for a receiver, the laser transmitter needs to send signals to all regions of its field of view. The number of locations the laser must search can be quite large if the divergence of the laser is small. Figure 12 shows a diagram of a laser searching over a field of view. The field of view is w in width and l in length. The half width divergence angle of the laser, δ, determines the size of the illuminated section at a distance of r.

With these variables, the total area illuminated by the laser at a distance of r is:

$$A = 4\delta^2 r^2. \quad (5)$$

The total number of locations, N, needed to exhaustively search the entire field of view is the division of the total search area by the spot size of the laser:

$$N = \frac{lw}{A} = \frac{lw}{4\delta^2 r^2}. \quad (6)$$

The field of view can also be defined by the angles defined as $\alpha = l/r$ and $\beta = w/r$; provided l,w<<r.

$$N = \frac{\alpha\beta}{4\delta^2}. \quad (7)$$

For example, in COTS Dust, the angular deflection of the mirrors is 14 degrees (0.25 radians) half angle in each direction, and the laser has a half-angle divergence of 2.5 milliradians. Using the above equation, the laser transmitter needs to signal 10,000 different locations to exhaustively search for an available receiver. If an imaging receiver is limited to 30 bps, one full second may be needed to transmit a complete packet. An exhaustive search can take 10,000 seconds or 2.7 hours to complete.

However long the acquisition step takes, once two devices know their partner's relative location, communication can be established without a spatial search. Additionally, the small divergence of the laser beam minimizes the total output power needed to communicate. The following section compares optical communication with RF communication and discusses the relative advantages and disadvantages between the two.

2.4.4 Optical Communication vs. RF Communication

A few points should be noted in regards to the differences between optical and RF communication. Both forms of communication are based on sending electromagnetic waves through air. While an RF wavelength can range anywhere from 30 meters to 1 cm, an optical wavelength is about six orders of magnitude smaller, ranging from 700 nm to 350 nm.

As quoted from Stephen Lambert in his book, *Laser Communications in Space* [17]: "From scalar diffraction theory, the angular divergence of a plane wave spatially filtered by an aperture of diameter, a, is proportional to the wavelength, λ, and inversely proportional to the aperture size."

$$\theta_{div} = \frac{4\lambda}{\pi a}. \quad (8)$$

For a laser beam at 670 nm with a lens of one millimeter, the limiting divergence is 853 μradians. If we wanted an RF signal of 1 GHz to have a divergence of only 1 radian, the limiting aperture would have to be 30 centimeters in diameter. While it is possible to focus a laser beam to a very small divergence angle, RF waves generally propagate isotropically on COTS Dust scale, that is isotropically from the source. Ignoring atmospheric effects, if an RF wave is being generated at a point source, uniformly propagating in all directions, its power density is determined by:

$$S(r)_{density} = \frac{P}{4\pi r^2} \text{ where p is the power and r is the distance from the source.} \quad (9)$$

A laser's power density, on the other hand, is inversely proportional to the solid angle carved out by its divergence, Ω:

$$S(r)_{density} = \frac{P}{\Omega r^2}. \quad (10)$$

If a laser has a divergence of 1 milliradian, then the solid angle, Ω, carved out of the unit sphere would be 10^{-6}. The power density would be ten million times more than that of an RF transmitter with the same output power.

Clearly, the small divergence angle allows lasers to transmit information at lower

powers than RF. Nevertheless, to fully compare RF to optical communication one must also take into consideration the receiving end of the communication system. For both RF and optical communication, there is a trade-off between size and receiver performance. For RF receivers, antennas need to be on the order of λ to reduce radiation loss., and for optical receivers, a lens can increase the amount of light directed into the photodiode proportional to the area of the lens. Receiver sensitivity and lighting conditions can also affect the performance of the optical receiver. Intrinsically, the receiver's sensitivity can be limited to shot noise of the diode, diode size, and receiver bandwidth. RF communication has another set of factors to consider. The antenna design, surrounding RF environmental noise, and receiver sensitivity affect the performance of the RF system. Modern cellular phones can obtain an RF receiver sensitivity of -100 dBm, and Leibowitz [18] is designing an optical imaging receiver for Smart Dust with a receiver sensitivity of -50 dBm. It is important to keep in mind that the performance of the overall system depends on both the transmitter's and receiver's capabilities.

3.0 COTS Dust Systems

Based on the architectures described in Section 2.0, I designed and built several unique systems (see Figure 13). The descriptions of each COTS Dust system are outlined below. To give the reader an idea of the functionality, each section describes a demonstration of the device's capabilities. Here, I point out the interesting design challenges that arose while making a fully operable system. The sections are ordered chronologically according to when I designed and built each system.

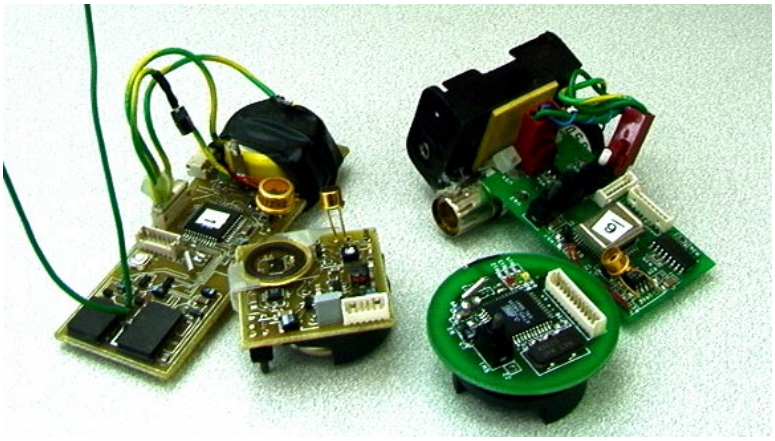

Fig. 13. COTS Motes. From left to right: RF Mote, CCR Mote, weC Mote, Laser Mote.

3.1 Mouse Collars

Working with Karen Nutt [19], I designed light collars that were used in nocturnal behavioral observations in the wilderness at Hastings Natural History Reservation. The goal of the research project was to provide a means of locating mice that lived on the reservation. By affixing a collar around the necks of the mice, Nutt was able to remotely illuminate the LED on the collar using a wireless radio link (see Fig. 14 and Fig. 15 on page 36). During the night time, one could locate the mouse from the illumination of the

LED and thus obtain the mouse's approximate location.

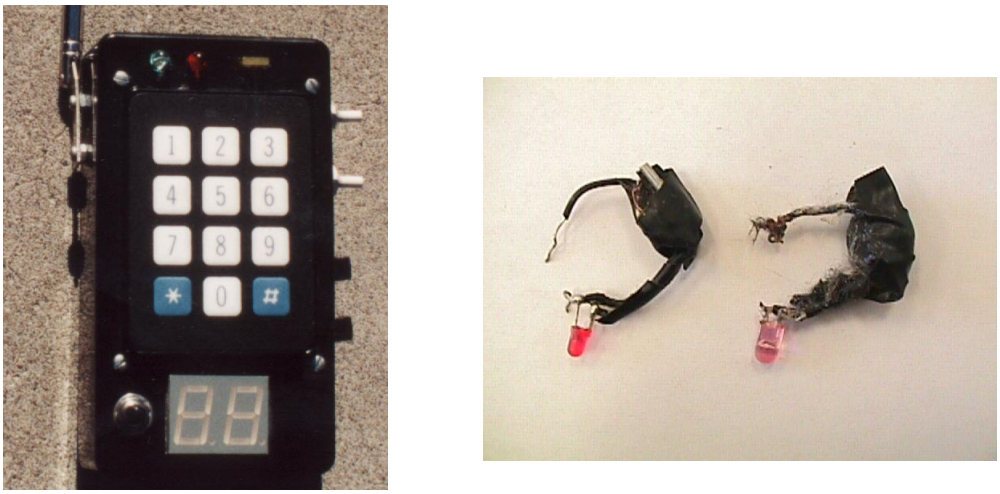

Fig. 14. Transmitter and Mouse Collars. Transmitter is used to turn the collars on and off. Collars are approximately 2 inches in length.

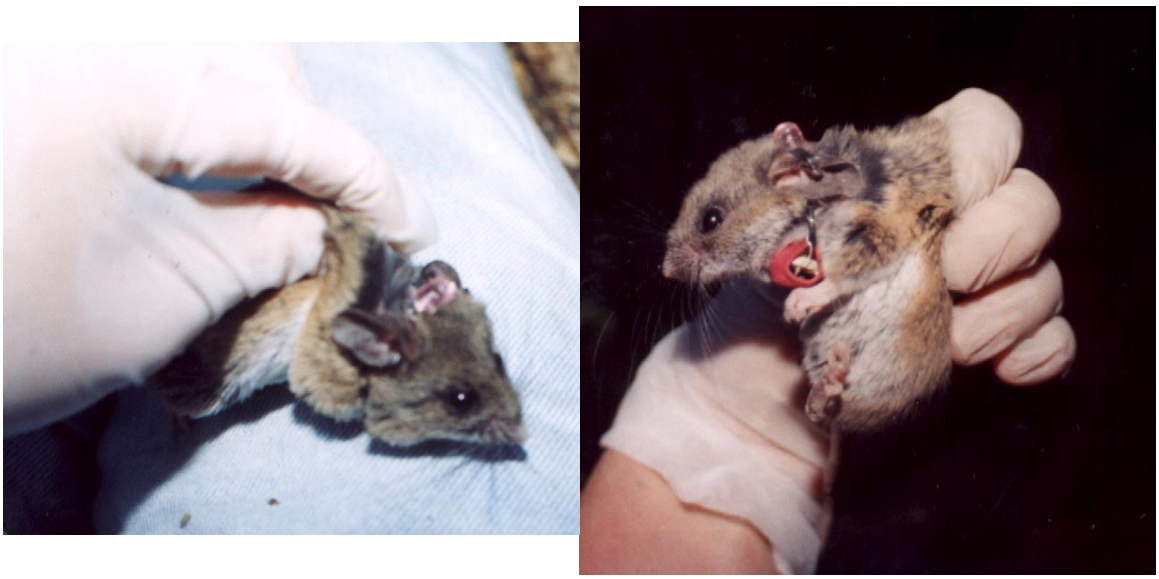

Fig. 15. Mouse and LED collars. Note: Mouse collars in pictures do not contain RF receivers.

The collars included an RF receiver, microprocessor, and LED. They weighed approximately 3.3 grams and could be turned on remotely from up to 50 meters away.

The battery weighed about one gram, and assuming average use, the collars had a one month lifetime.

Power consumption was a major consideration in designing the light collar. The Microchip PIC12C509 ran at 32.768 KHz where most instructions were executed in 4 clock cycles, allowing 8192 instructions per second. While computationally slow, the MCU consumed 15µA at 3 Volts. The MCU's main function was to maintain a real time clock and listen for signals coming in from the receiver. The receiver, consuming 1.2mA of current, was turned on for only 50 ms every 5 seconds to conserve power.

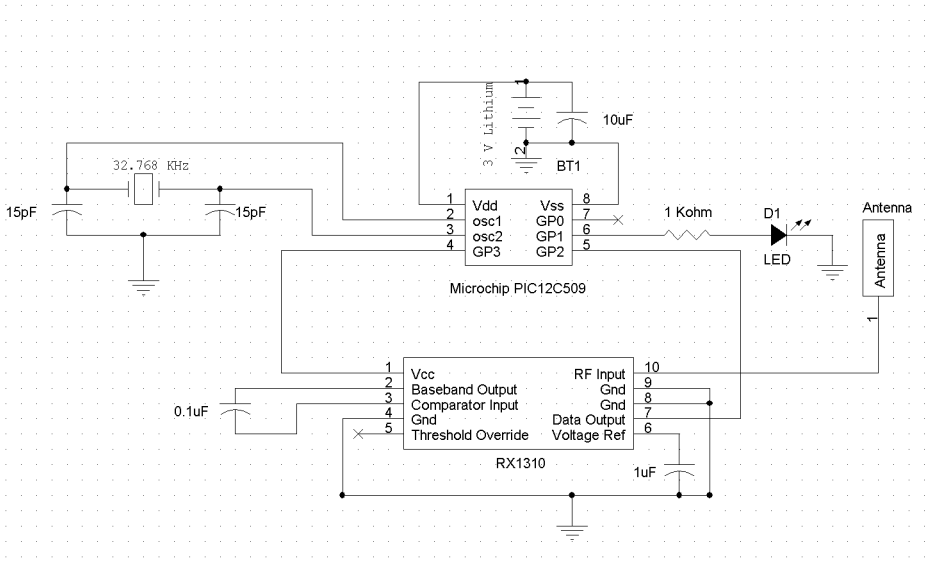

Fig. 16. Mouse Receiver Collar Circuit Diagram.

The RX1310 received modulated signals based on OOK. The MCU's job was to 1) detect a bit stream 2) synchronize with the bit stream, and 3) capture the first 16 bits. Because the MCU ran at 8196 instructions per second and the software needed 6 instructions per bit to capture data, the throughput of the receiver was set at 8192/6 bps or 1365 bps.

Each LED collar could be turned on individually, implying a unique code was assigned to each collar. Should the code match that of the collar, its LED would turn on. A two byte code was chosen for each ID, but additionally, the total number of possible codes was limited based on the receiver specifications. For one, the receiver needed a DC balanced signal (i.e. a roughly equal number of ones as zeros). To ensure transitions in the bit streams, I required the ID code to have no more than 3 continuous zeros or ones.

Lastly, the receiver stayed on only long enough to capture 16 bits of information, regardless of when the transmitter started sending data. To accomplish this, the transmitter sent out the two byte unique ID continuously. On the receiving end, the MCU would circularly rotate the captured bits 16 times, each time looking for a matching ID (see Fig. 17 on page 39). Since each unique code had to be circularly permuted, no two ID codes could be circular permutations of one another.

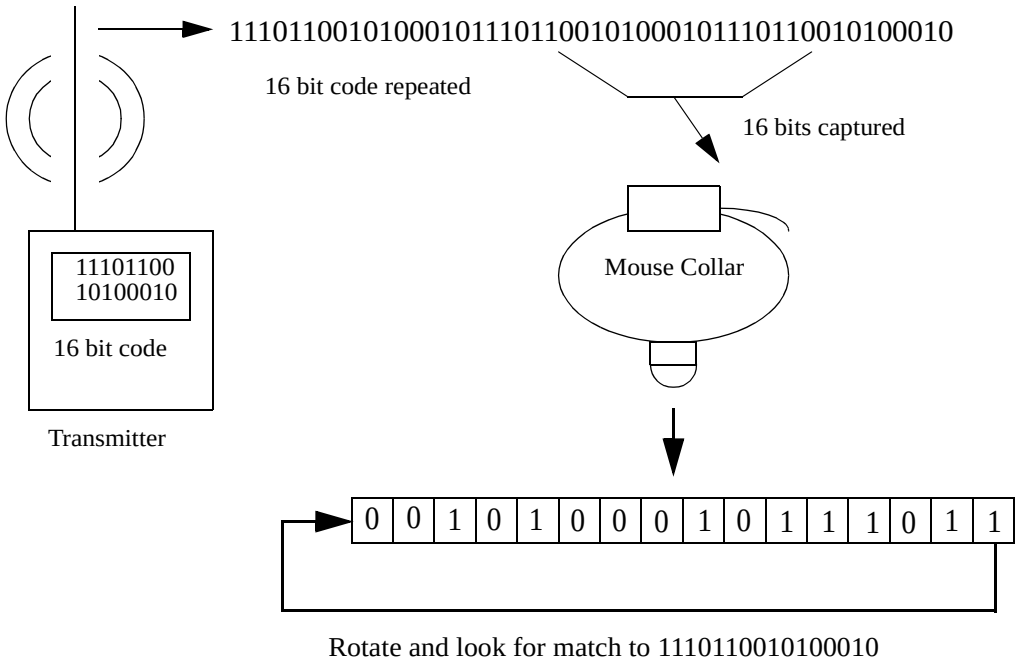

Fig. 17. Collar Communication Diagram. Transmitter sends out consecutive sequence of a 2 byte code. Receiver receives 16 bits, and rotates the bits, looking for a match to its ID code.

With these constraints, I was able to ensure a DC balanced signal and allow for quick recognition of a unique ID code. In all there are 350 unique ID codes possible from a two byte code. Each collar accepted three unique commands: 1) flash LED, 2) turn off LED, and 3) go into power save mode. Thus, a total of 350/3= 116 unique ID collars was possible under this configuration. Of course, if I increased the length of the unique ID code I could increase the total number of codes.

3.2 Radio Frequency Mote (RF Mote)

The RF mote follows the architecture found in Fig. 1 on page 8. The autonomous sensor mote consists of the Atmel AT90LS8535, an RF Monolithics 916MHz transceiver

set, and 7 sensors (temperature, light, barometric pressure, 2-axis acceleration, and 2-axis magnetometers). A single 3-V lithium coin cell battery powers the mote, sustaining either five days of continuous operation or 1.5 years at 1% duty cycling. See Fig. 18 on page 40 for a commented picture of the RF mote. Unlike the CCR motes, the RF motes can communicate wirelessly with one another where reliable RF communication has been demonstrated at distances ranging from 5 to 30 meters.

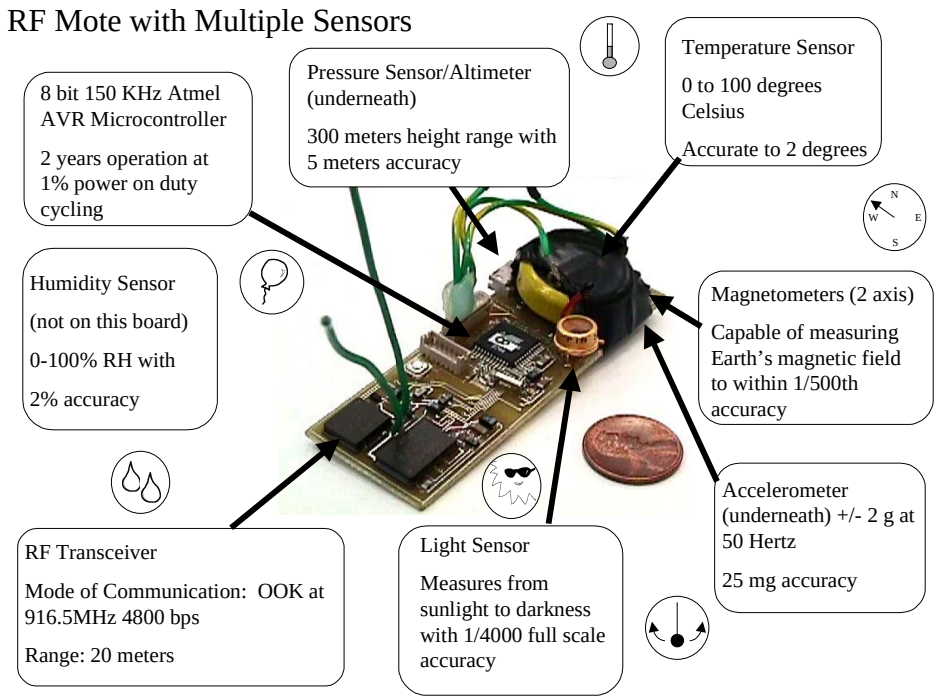

Fig. 18. RF Mote. Captions indicate the various subsystems of the RF Mote.

Since the transceivers operate at a single carrier frequency, 916 MHz, only one device can transmit at a time. If two devices transmit, collisions can occur causing the data to become unreadable. Additionally, especially in noisy environments, packets of data can be corrupted during transmission. While there is no protocol in place for retransmitting lost data packets, cyclic redundancy check (CRC) was implemented to check

packet integrity. The simple demonstrations in sections 3.2.2 and 3.2.3 are examples that show the utility and capabilities of distributed sensor networks. In addition, they provide simple solutions for transmitting data with relatively few collisions.

3.2.1 RF Communication

The system clock of the Atmel MCU runs at 149.475 KHz with a single instruction performed per clock cycle. Nineteen instructions are required to send and receive raw data bits through the RF system. The raw data rate of the RF system is 149.475 KHz/ 19Cycles/bit = 7.867 Kbps, but with the implementation of manchester encoding, the data rate is cut in half to 3.934 Kbps.

In programming the RF motes, I implemented an operating system where processes were performed serially. While this method of programming is easier to implement than multi-tasking systems, only one process can be run at a time. For example, the processor can measure the acceleration or transmit data but cannot do both simultaneously.

3.2.2 Acceleration Sensing Demonstration

An example of how the RF motes could be used is described in the following scenario. Imagine that the RF motes were placed by a highway. When a car drives by, the road would vibrate from the rumblings of the vehicle. Both the amplitude and frequency of these vibrations might reveal information about the size and speed of the vehicle. RF motes equipped with accelerometers could then monitor the highway, continuously measuring amplitude and frequency of the vibrations. Suppose now, that we wanted to detect only very large trucks on the highway. The RF motes could analyze the strength of vibrations. Should the signal strength exceed a certain threshold, the RF motes would deduce

that a large truck drove by and alert neighboring motes.

I implemented a simplified version of the above scenario using three RF motes. The RF motes would contact neighboring motes if they sensed large changes in acceleration (see Fig. 19 on page 42). If accelerated, an RF mote would transmit a distress signal to neighboring motes. The distress signal would be in the form of a simple data packet containing the unique ID code of the mote. Neighboring RF motes receiving the distress signal would blink with their LED. Though simple, this particular demonstration is a good example to look at collisions and ensure adequate communication on the single RF channel.

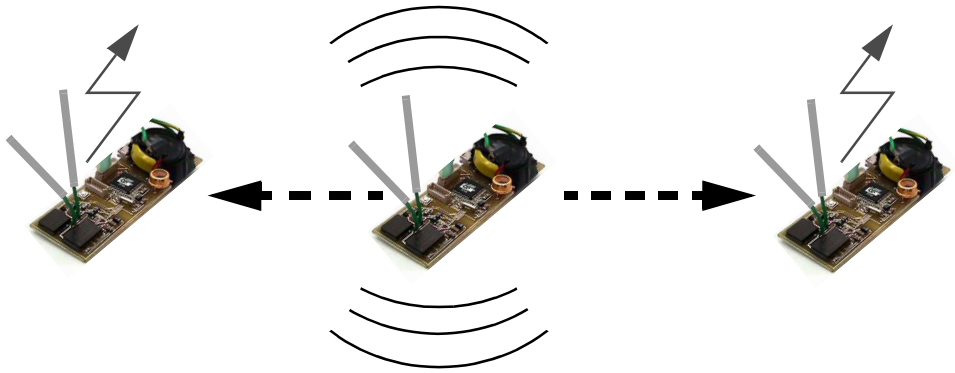

Fig. 19. The Acceleration Sensing Demonstration. This demonstration showed how sensors and RF communication could be used to detect motion and alert neighbors. When the RF motes detected acceleration, they would transmit their ID over RF. Motes within communication range would receive the signal and flash the accelerated motes' ID from their LED.

The algorithm of the mote has two basic functions which occur one after the other. First, the mote measures acceleration, and second, the mote listens for distress signals from other motes. Because operations work serially in the microprocessor, the mote cannot listen for distress signals while it measures acceleration and vice versa. The mote spends 16 ms measuring acceleration and 100 ms listening. If the mote hears no distress signal, it simply starts over, first measuring acceleration and then listening for a signal.

The timing diagram can be seen in Block A of Fig. 20 on page 43.

Block B shows when a valid a transmission needs to start if the RF mote is to receive a valid distress signal. The total time to listen for transmissions and measure acceleration is 16 ms + 100 ms = 116 ms, while the regime for valid transmission starts is from 14ms to 104ms. That implies, that there is a period of 90 ms out of 116 ms where a valid reception can occur. Provided the motes are uncorrelated in time, the chance that the mote will detect a transmitted signal is 90 ms / 116 ms = 78% per cycle. The valid start regime (14 ms) starts 2 ms before the listening regime (16 ms) because the training sequence consumes a few milliseconds of time in the data packet (see page 27).

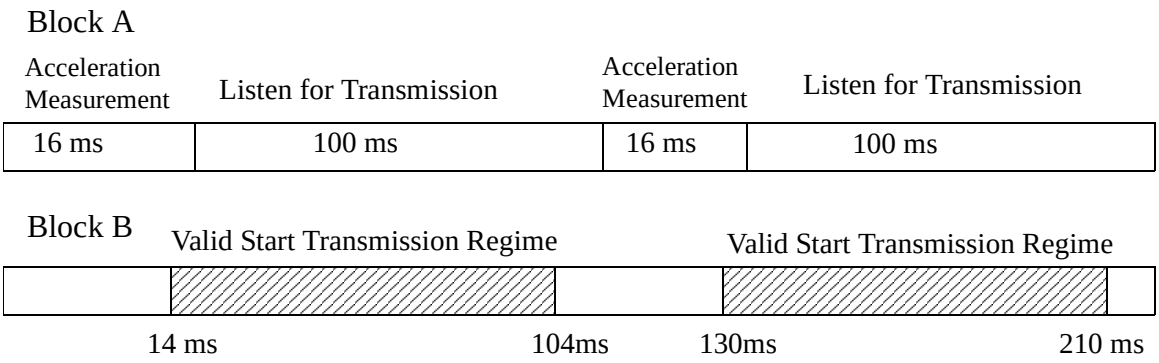

Fig. 20. Timing Diagram for Valid Communication Regimes. The RF motes read measurements for 16 ms and then listen for a signal for 100ms. A valid transmission regime for another mote encompasses about 90 ms in one cycle.

Depending on the application, 78% might be adequate, but in other cases it is not. Two ways to improve the reception rate is 1) to increase the listening time of the device or 2) implement an event driven system where the receiver is continuously listening. In the former, the frequency of acceleration measurements is decreased. The latter situation requires more careful consideration. Hill *et al.* have addressed this problem and others in their TinyOS operating system [20]. At a data rate of 3.934 Kbps, the processor is already

dedicating 100% of its time transmitting and receiving. In order to implement a multitasking operating system, the MCU must have some free time during RF communication. Two possible solutions would be to either generate a faster processor clock or reduce the data rate of the RF system.

3.2.3 Single Hop Sensor Retrieval Demonstration

Often times, it is not only necessary for COTS Dust to communicate with one another but also to communicate outside of the network. In this demonstration, sensor data is retrieved from remote devices and displayed on the computer. This is an example of how RF motes can successfully communicate with one another and sustain prolonged periods of data transmission. Single hop communication is demonstrated, and later in this section, RF synchronization issues are discussed.

In single hop communication, information is sent from one device to the next through one RF transmission-reception pair. For this demonstration, there are two types of motes (see Fig. 21 on page 45). The base mote communicates to the computer via the serial port, and the floating motes communicate to the base mote via RF. The user can specify which motes and additionally which sensors to query. Should the floating mote be within RF range of the base mote, the data can be retrieved and viewed on the computer.

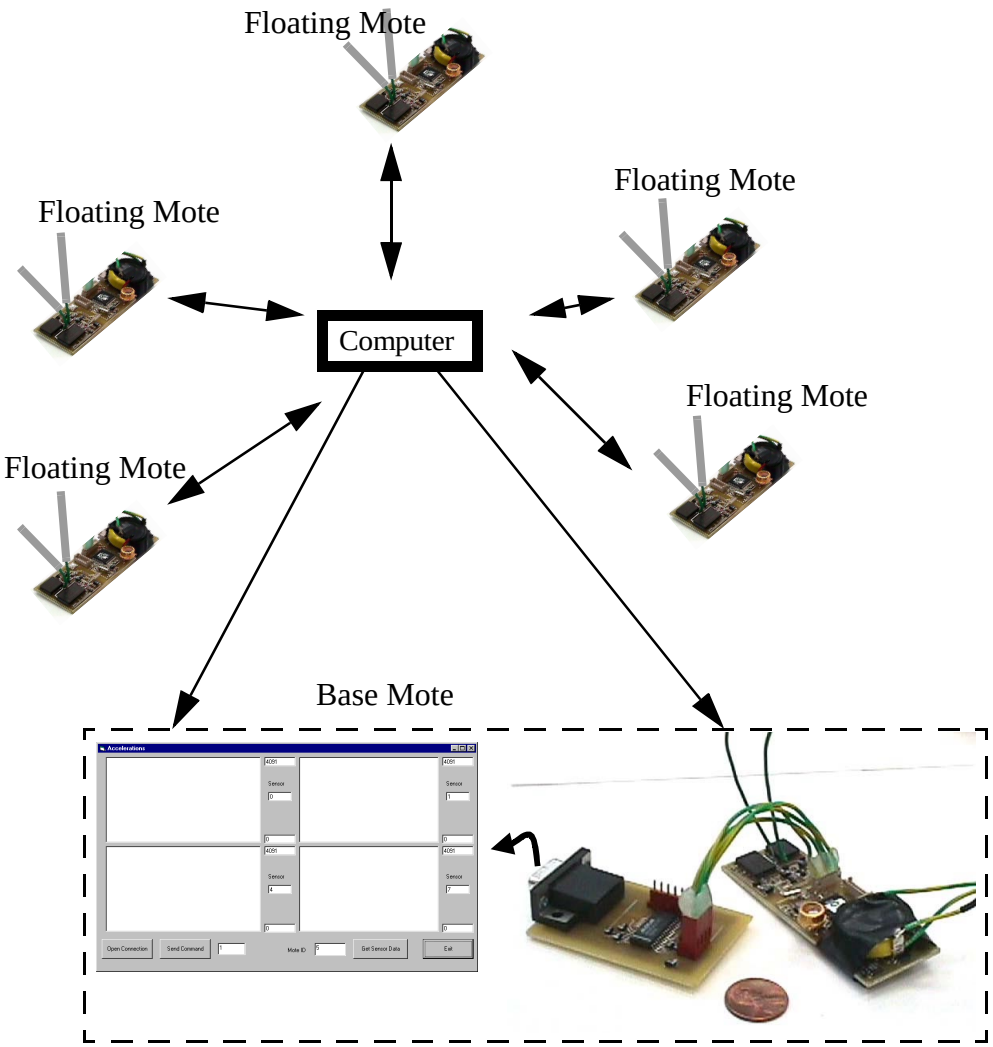

Fig. 21. Single Hop Sensor Retrieval Demonstration. Motes can be queried by the computer for sensor data. Software on the computer takes that data and plots it over time.

3.2.3.1 Synchronized Data Flow

When transmitting data, the floating motes send out data packets constantly. The packets are received by the waiting base mote which displays the information on the computer screen. The timing of packet transmission is synchronized between the two devices to optimize data throughput.

To establish synchronization, the base mote must first query one of the floating

motes. According to the protocols in Fig. 22 on page 46, the base mote sends out a transmit query and listens for a response. If a response is not heard after 100 ms, it proceeds to send out another transmit query. The base mote repeats the algorithm until a valid message is received. Once received, the message is sent from the base mote to the computer over the serial port. The base mote then proceeds to listen for the next packet of data.

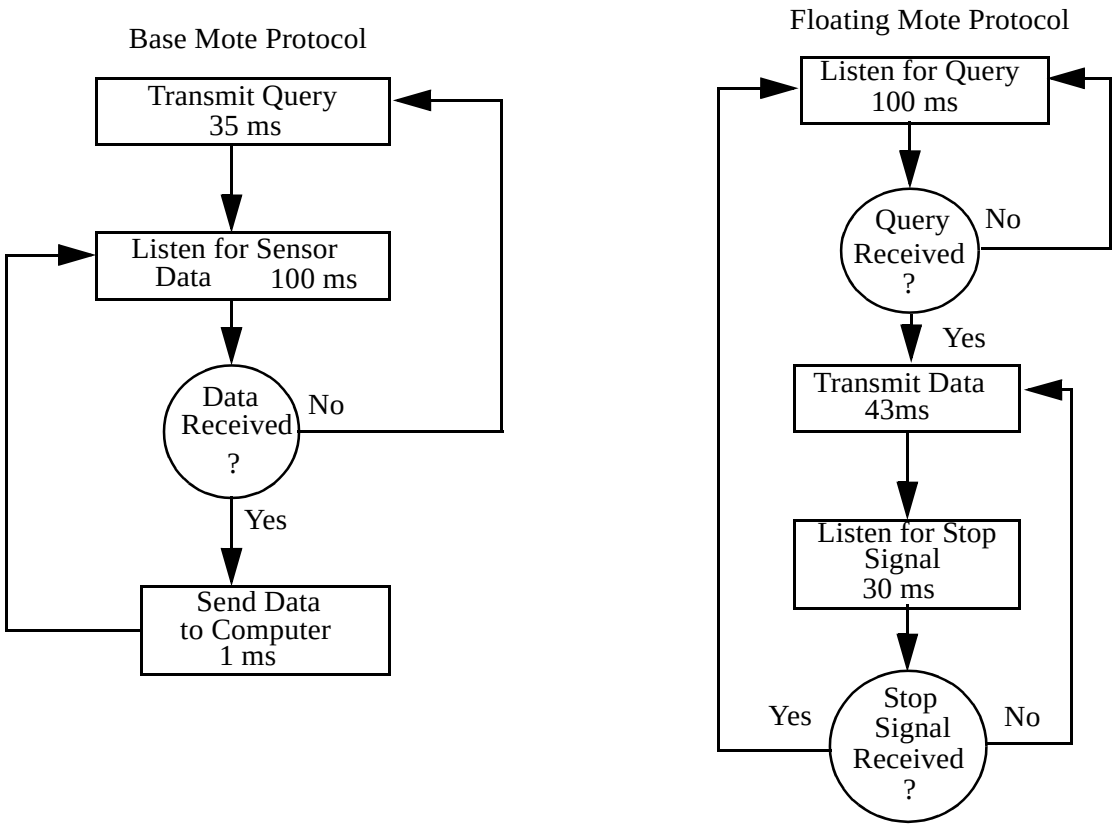

Fig. 22. Protocols used for Base and Floating Mote. The base mote transmits a query and listens for received signal. If no signal is received, it retransmits. The floating mote continuously listens for a signal. When a valid signal is received, it transmits its sensor data continuously while listening for 30ms in between transmission.

Likewise, the floating mote listens for a query. Once a query is received, the floating mote transmits sensor data to the base mote. The transmission takes 43 ms to com-

plete. Afterwards it listens for 30 ms, if no signal is received, it transmits, again.

Both protocols above have listening periods right after transmission periods. This enables motes to respond to queries right away. The handshaking enables both motes to communicate with one another as quickly as possible. Furthermore, the motes have synchronized communication channels.

In order to synchronize, however, the motes need to make an initial communication. In the section below, I will discuss an example that points out the factors involved in establishing communication between uncorrelated motes.

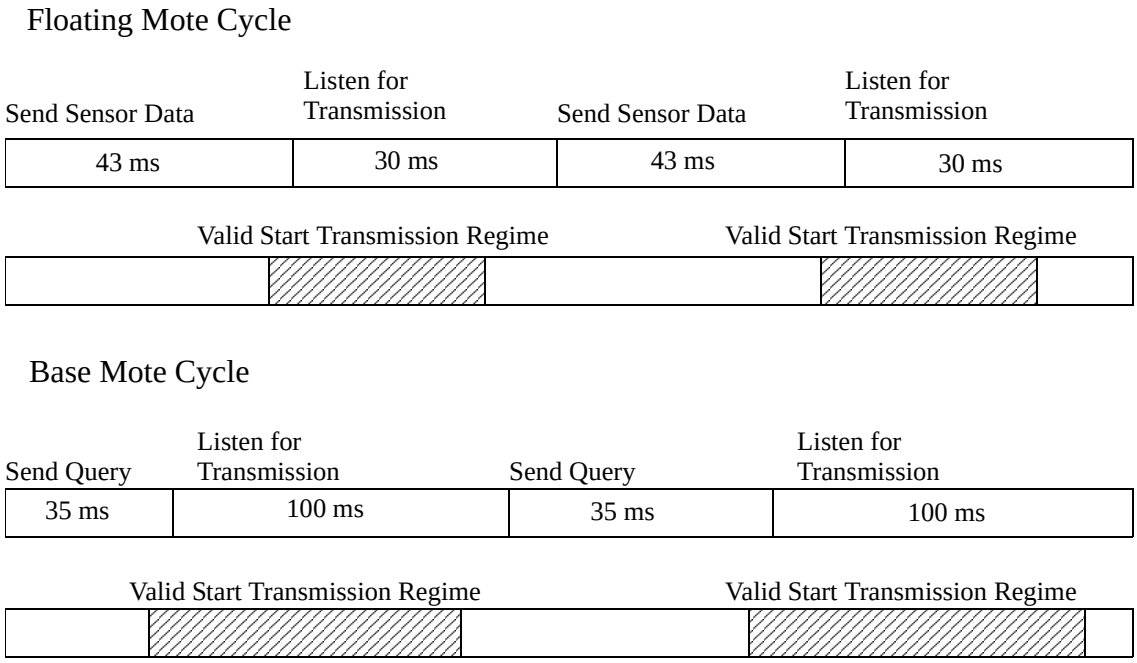

Fig. 23. Valid Transmission Regimes for Base and Floating Motes. The long listening times for the base mote coupled with the short transmission times of the floating mote, make it easy for the two motes to become synchronized.

3.2.3.2 Establishing Communication Links

Suppose that a floating mote is repeatedly sending data. The base mote, not syn-

chronized to the floating mote, would like to terminate the floating mote's transmissions by transmitting a stop signal. How long will it take the floating mote to receive a valid stop signal?

The base mote follows the same protocol to send a stop signal as it does to send a query. The base mote sends for 35 ms and then listens for 100 ms (see Fig. 23 on page 47). Likewise, the floating mote transmits for 43 ms and listens for 30 ms. The chance it takes the floating mote to receive a stop signal, follows the equation below:

$$P_{tot}(t) = 1 - (1 - P_{base}(t - 35ms))(1 - P_{float}(t)). \quad (11)$$

where $P_{tot}(t)$ is the total probability the floating mote has received a stop signal.
$P_{base}(t)$ is the probability an initial message is received by the base mote.
$P_{float}(t)$ is the probability an initial message is received by the floating mote.

An extra 35 ms is added on to the probability of P_{base} in Equ. 11 to account for the time it takes to send a stop signal to the floating mote.

For the floating mote, the total cycle period is 30ms + 43ms = 73 ms, where 20 ms is the valid start transmission regime. For a given transmission the chance of reception is 20 ms / 73 ms = 27%. Likewise for the base mote, there is a 67% chance of reception. Fig. 24 on page 49 shows the theoretically calculated probability of reception.

Notice how P_{base} contributes most to P_{tot}. This implies that the base mote will most likely receive a valid transmission from the floating mote before the floating mote receives a stop signal from the base mote.

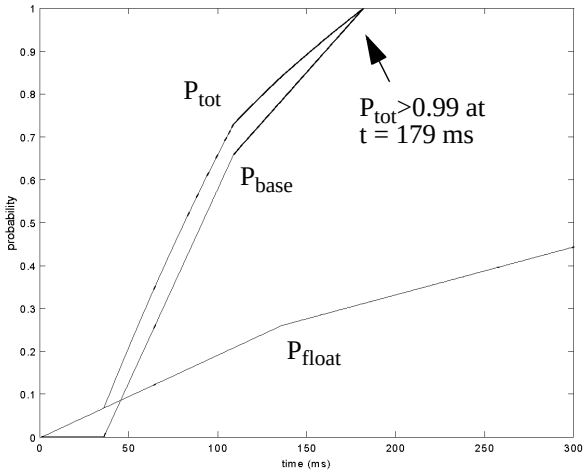

Fig. 24. Theoretical Probability of Reception. P_{tot} reaches 0.99 after 179 ms.

P_{base} is maximized when its probability of reception is maximized and the interval between transmissions of the floating mote are minimized. While the floating mote has a very low probability of reception, it does however have a high transmission frequency. That coupled with the long listening periods of the base mote maximize the probability that both motes will be able to establish communication in a short time frame.

3.3 Laser Mote

The laser mote, otherwise known as the miniature weather station, is a fully autonomous mote (see Fig. 25 on page 50) that uses active laser communication to send sensor data long distances. The laser mote ran off 2 AA batteries and contained four sensors: humidity, light, temperature, and pressure. A laser module from a handheld laser pointer served as transmitter. Mounted directly on the laser mote, the laser module had to be manually adjusted to point towards the receiver. The standard Atmel 90LS8535 microcontroller served as the computation subsystem, while the Dallas Semiconductor alarm chip allowed the laser mote to go into low power mode (~1 μW).

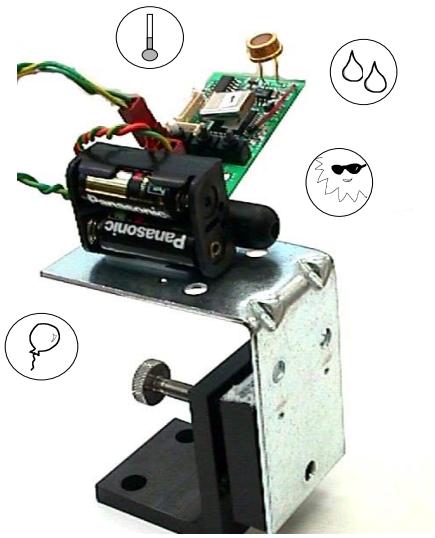

Fig. 25. Laser Mote. The Laser Mote contains four sensors: humidity, light, temperature, and pressure.

3.3.1 One-way Asynchronous Laser Communication

To demonstrate the long range capabilities of laser communication, UC Berkeley graduate student, Matthew Last, placed the laser motes in various locations around the San Francisco bay area [21]. A diagram of the system can be seen in Fig. 26 on page 51. At the Berkeley Marina, a laser mote was positioned so that the laser was pointing towards the camera some 5 km away. I programmed the laser motes to read and transmit weather data every three minutes. In general, the laser motes would be in low power mode for two minutes and transmit sensor data the third. Transmission took one minute due to the extremely low data rate, 4 bps.

The imaging receiver used in the laser communication system is a CCD camera interfaced to a laptop computer via a high-resolution frame grabber. Identical software to that used in the CCR demonstration (Fig. 34 on page 60) was used to decode signals from the laser mote [22]. The camera ran at 30 frames/second, while the computational power

of the laptop further limited the data rate to 4 bps. However, data rates in excess of 1 kbps are possible using commercially available high-speed cameras.

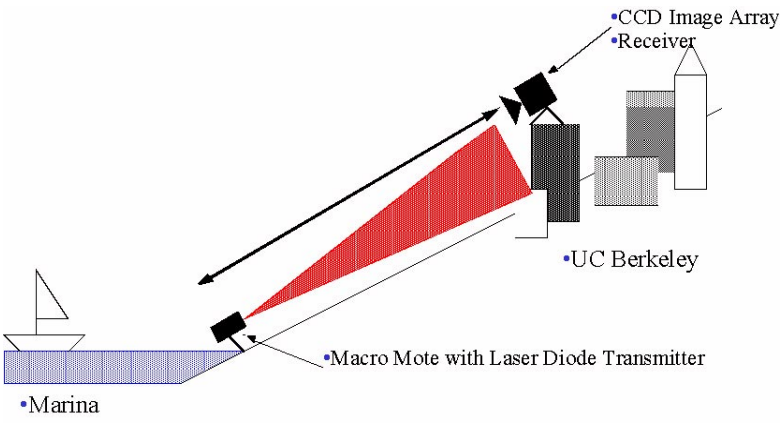

Fig. 26. Bay Area Laser Communication. . Laser mote is placed by Berkeley Marina and aimed in direction of CCD Image array 5.2 Km away. The laser mote temperature information back to the receiving information by OOK at 4 bps.

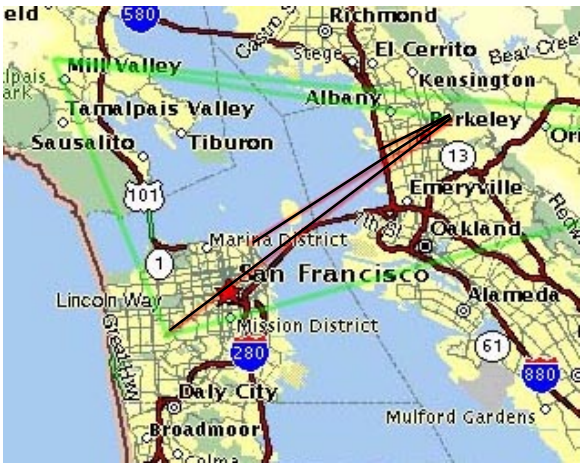

Fig. 27. Laser Mote Cross-Bay Communication. The black lines represent the path of the laser during the laser communication. Three experiments were run with the longest successful range being 21.4 Km.

Last demonstrated repeatable weather data transmission from three different locations: A) from the Berkeley Marina to Cory Hall at UCB (5.2Km), B) Coit Tower in San Francisco to Cory Hall (15.3km), and from Twin Peaks in San Francisco to Cory Hall

(21.4 km) (see Fig. 27 on page 51).

3.4 Corner Cube Reflector Mote (CCR Mote)

The CCR mote, codesigned with Farrah Santoso, communicates to other devices using passive laser communication by means of the corner cube reflector (see "Passive Laser Communication" on page 28). The CCR mote is the first COTS Dust designed with a custom designed integrated MEMS device on board.

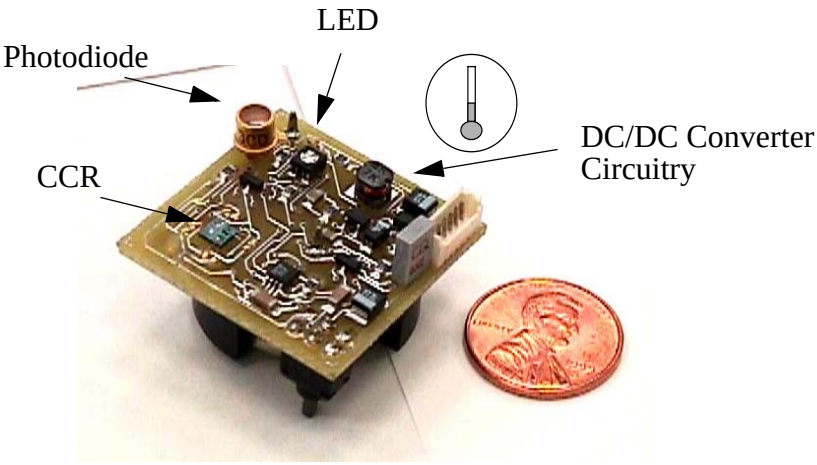

Fig. 28. Corner-Cube-Reflector Mote.

The CCR mote was designed to mimic Smart Dust as described in the scenario of "Enemy Troop Monitoring" on page 3. As seen in Fig. 17 on page 39, the interrogator queries CCR motes by sending a diverged laser signal in the approximate direction of the devices. The motes receive the signal and depending on the nature of the command, return temperature data. The laser beam from the interrogator is reflected and modulated by the CCR in the form of binary data. The data is then decoded back into the motes' temperature information.

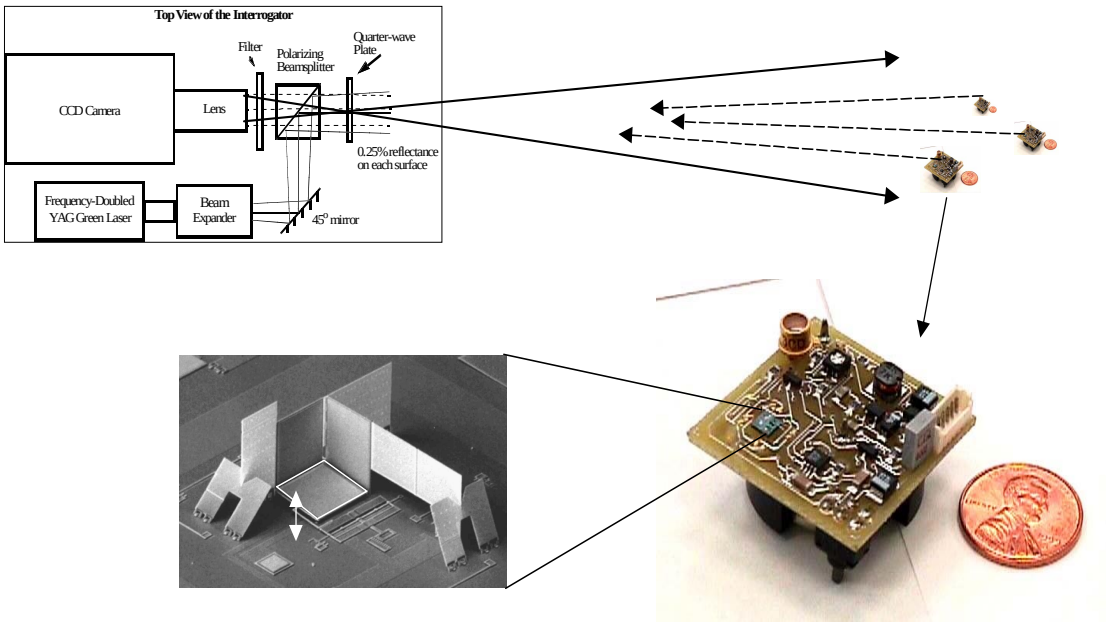

Fig. 29. Laser Interrogator Querying CCR Mote. The beam of theYAG green laser reflects off the beam splitter to the CCR motes. The CCR motes reflect back their signal through the beam splitter into the CCD Camera. Software is used to process the flashing signals into valid data.

3.4.1 CCR Mote Architecture

The optical communication of the CCR mote can be categorized into 1) the CCR uplink and 2) the photodiode downlink. The CCR uplink transmits information from the CCR mote to the laser interrogator system. More specifically, it provides for the optical reflection and mechanical actuation of the physical corner cube reflector. The CCR and an associated DC/DC converter are the components of the uplink. A DC-DC converter is required to step the voltage up from 3 volts to 15 volts to actuate the electrostatic mirrors used in the communication of the CCR devices.

3.4.1.1 Photodiode Downlink

In the photodiode downlink, the CCR mote receives and decodes signals from the

laser interrogator. The design of the photodiode downlink was dictated by the requirements on the data rate and range of communication.

In designing the specifications for the CCR mote, the Smart Dust team wanted the device to operate both indoors and outdoors (see Table 7 on page 54). Not only would the device need to handle a large DC light bias from the sun (~1 kW/m^2), it would also have to filter out 60 and 120 Hz noise from fluorescent lighting. To accommodate both scenarios, analog front end circuitry was designed with a low and high pass filter. As seen in Fig. 30 on page 55, the incoming light signal is converted into a voltage with a transresistance amplifier. The signal is then high pass and low pass filtered where the filters are implemented by a Maxim 5 pole filter with a software adjustable corner frequency. Finally the signal is sampled by an A/D converter.

Table 7: Specifications for CCR Communication

requirements	specifications
laser intensity	5mW
laser divergence	0.05 radians half angle
minimum range	10 meters
environment	must work from full sunlight to indoor light include fluorescent light
data rate downlink	30 bps

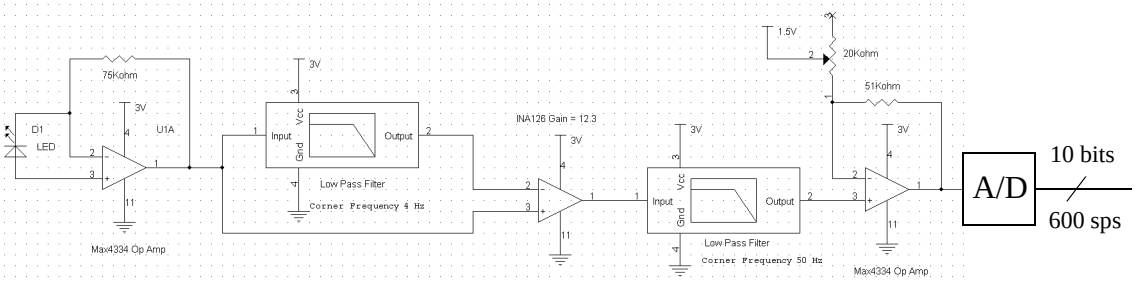

Fig. 30. Photodiode Receiver Circuitry.

To gain a better understanding of the noise from fluorescent lighting, I ran two experiments. In the first experiment, the corner frequency of the low pass filter was set to 40 Hz. I then generated a laser signal whose power density was set to the minimum specifications of the receiver, a power density of 5 mW/m^2. In the presence of normal fluorescent lighting I pointed the laser into the photodiode. I recorded the voltage at the output of the analog front end and graphed the fourier transform of the resultant signal (see Fig. 31 on page 56). As shown, the signal power is much larger than the 60 and 120 Hz from the fluorescent lighting.

The second experiment was a slight modification from the first. The corner frequency of the low pass filter was pushed up to 88 Hz, and the laser signal was generated at 100 Hz. As can be seen, the 100 Hz signal is swamped by the 120 Hertz noise. Without attenuation the fluorescent lighting would emit an average power density of 50 mW/m^2 at 120 Hertz, ten times stronger than the incoming minimum specified signal.

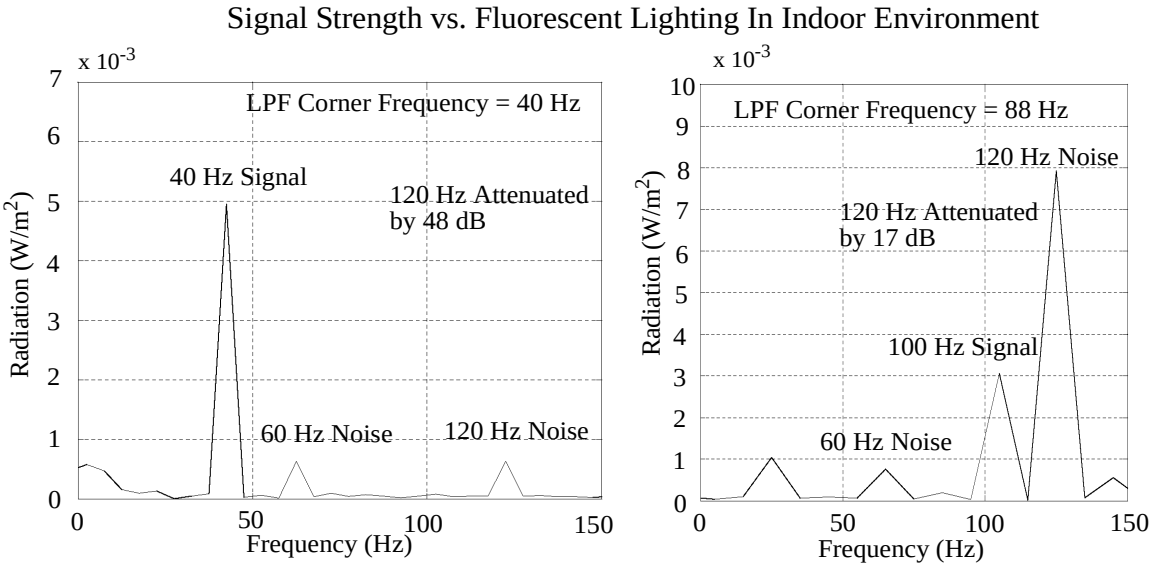

Fig. 31. Frequency Plot of CCR Receiver Signals and Noise. In the left plot, the LPF corner frequency is set at 40 Hz. The 40 Hz square wave signal is much larger than the 60 and 120 Hz noise. In the right plot, the LPF corner frequency is set at 88 Hz. The 120 Hz noise from the fluorescent lights dominates the signal.

Based on the results of the above experiments, I chose a communication protocol and data rate whose signal power was centered between 0 and 60 Hz. In order to significantly attenuate the 120 Hertz noise, I picked 50 Hertz as the corner frequency of the LPF, while the raw data rate of the signal was set to 60 bps.

In addition to high frequency noise sources, the signal is also affected by low frequency DC shift. Since the minimum signal power could be over 100 times smaller than the DC offset signal, even relatively small DC shifts can be significant noise sources. To kill two birds with one stone, so to speak, I implemented manchester encoding. As I mentioned before, the signal is sampled by an A/D converter after passing through the analog front end. After digitizing the signal, the Atmel processor can run simple signal processing techniques to further improve data detection. The transfer function to decode the Manchester signal depends on $\sin(\tau\omega/2)$ where τ is the raw data sample period (see Figure

Fig. 32 on page 57). Since τ is 1/60 s, $\sin(\tau\omega/2)$ has zeros at 0 Hz, 60 Hz, and 120 Hz. The zeros correspond exactly to the noise sources of the system, namely the DC sunlight and the AC fluorescent lighting. By implementing Manchester encoding, we have been able to mitigate the key noise frequencies of the system.

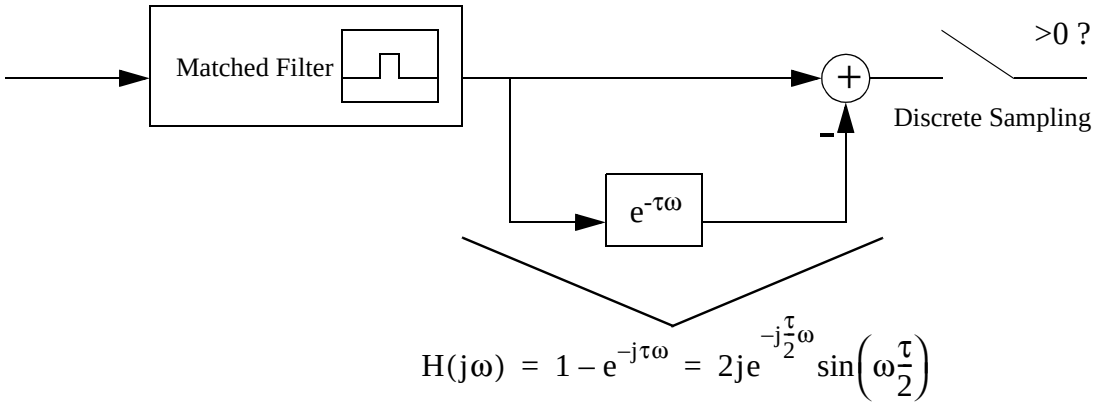

Fig. 32. Filtering Scheme for Manchester Encoding. A matched filter of a single pulse is followed by the difference of two consecutive pulses. The transfer function of the difference has zeros at 0, 60 Hz, and 120 Hz, for a raw data rate of 60 bps.

Without going into too much detail, the digital signal processing performed two tasks. The signal was digitized and processed with a DC running average filter and a matched filter. Secondly, a software phase locked loop (PLL) extracted the synchronized clock from the signal. The PLL relied on zero crossings to determine the phase of the system, making it sensitive to high frequency noise.

As an example, Fig. 33 on page 58 shows the state of the signal after the signal is digitized. Plot A shows the signal before the digital signal processing, and plot B shows the signal afterwards. Calculated zero crossings are marked by asterisks. Notice how after processing the signal has smooth zero crossings, whereas in the unprocessed state the zero crossings are more difficult to decipher. The matched filter significantly reduced the

noise where the signal crossed through zero.

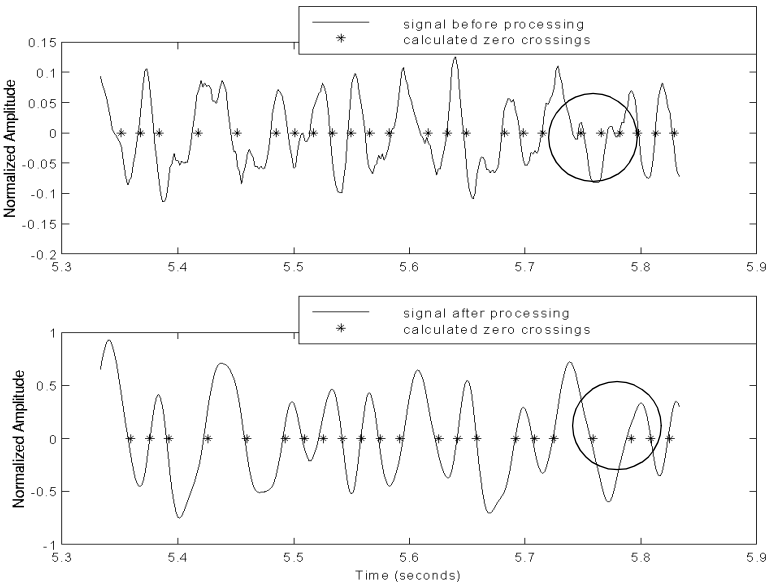

Fig. 33. Comparison of Signal before and after Processing. Plot A on the top shows the signal before a matched filter is applied. The circled region shows where zero crossings are not clearly resolved. Plot B on the bottom shows the signal after a matched filter is applied. Here, the signal shows clear transitions through the DC average.

3.4.2 Asynchronous Optical Communication with LED

To demonstrate the receiver uplink, I programmed the CCR mote to respond to laser interrogations (see Fig. 34 on page 60). The interrogator system is composed of a laser with diverging lens as its transmitter and a CCD camera and laptop as its receiver. By flashing the laser, the interrogator could transmit signals to the waiting CCR mote. Instead of using the CCR, the mote in this demonstration transmits back to the interrogator by flashing an LED. The interrogator would pick up the signal in the form of a flashing point on the CCD camera. Software from the laptop would then resolve the flashing point into valid data.

In particular, the laser interrogator transmitted signals that conformed to the receiver uplink protocol described in the previous section. Additionally, each CCR mote contained a unique identifier (mote ID). The interrogator system specified the mote ID and the number of temperature data points when querying the field. If the CCR mote happened to be within communication range of the system, it could communicate back the temperature data. With this system in place and a laser transmitter, successful two-way communication was demonstrated at a range of 9 meters.

The system could operate at a larger range if an optical filter was placed on the photodiode. A 50 nm optical filter on the photodiode could eliminate unwanted light from the solar spectrum improving the SNR by as much as 7-fold. In free space the power density of a diverged laser falls as the inverse square of the distance from the source. If 9 meters was the maximum communication range before the filter, 23.4 meters would be the range after the filter.

In Fig. 34 on page 60, the flashing LED signal is resolved by a CCD camera attached to a laptop computer running custom software. The software, written by Brian Fisher, looks for flashing signals that follow the appropriate communication protocol. With a 16 bit CRC, there is less than a 0.01% chance that random flashing lights would generate a valid signal.

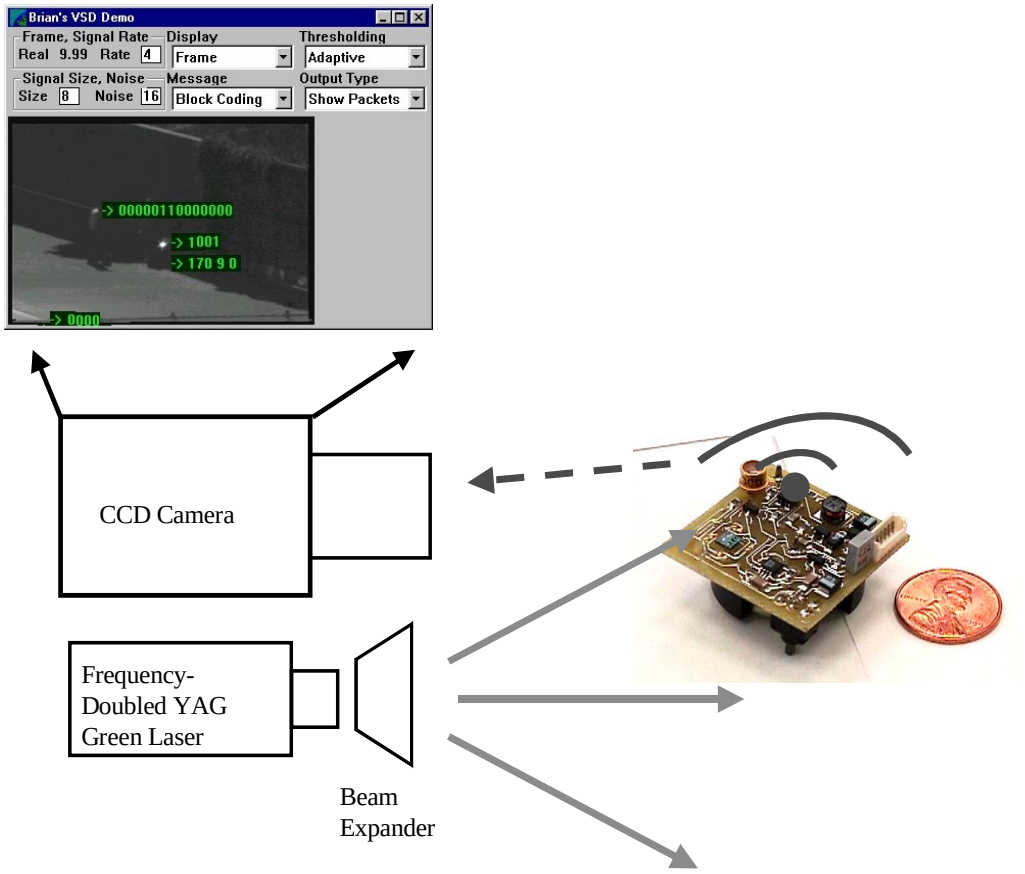

Fig. 34. Two-way Asynchronous Optical Communication with Laser Interrogator and LED. The interrogator sends a query signal to the CCR mote by means of the YAG green laser. By flashing its LED, the CCR mote sends back temperature data. Software connected to the CCD camera decodes the blinking lights into coherent data. Note picture in software is not from this demo.

3.5 Miniature Motes

The minimotes are basically smaller versions of their predecessors, the RF motes. Co-designed with Christina Adela, the first minimote contained an RF transceiver, temperature sensor, and Atmel AVR AT90S2313, a smaller version of the AT90S8535. Measuring approximately 1”x1”x0.5”, it is to date the smallest fully functional COTS Dust designed (see Fig. 35 on page 62).

The second version of the mini motes is called the weC mote, which was designed with James McLurkin (see Fig. 36 on page 62). The original intent of the weC mote was to test out algorithms specifically mentioned in his thesis [23]. The weC mote measures a bit larger in size but has a number of additions. In addition to an integrated PCB antenna, the weC mote contains both light and temperature sensors. With a CPU clock of 4 MHz, the weC mote is also the most computationally powerful of the COTS Dust. However, the real advantage behind the weC mote is that the hardware configuration supports remote reprogramming of the Atmel chip. Essentially, this allows the weC mote to be reprogrammed over a wireless link, whereas all previous versions of COTS Dust must be programmed through a connector.

Work with the weC mote is being continued with Endeavor. Endeavor is a team of CS researchers in UC Berkeley who are attempting to improve interaction between information, devices, and people in the post-PC computing era [24]. Hill *et al*. have developed an operating system, TinyOS, for the management of different functions on board the weC [20]. Additionally, in the spring semester 2000, graduate class CS294-8 under Professor David Culler in UC Berkeley used the weC motes as hardware for developing networking algorithms [25].

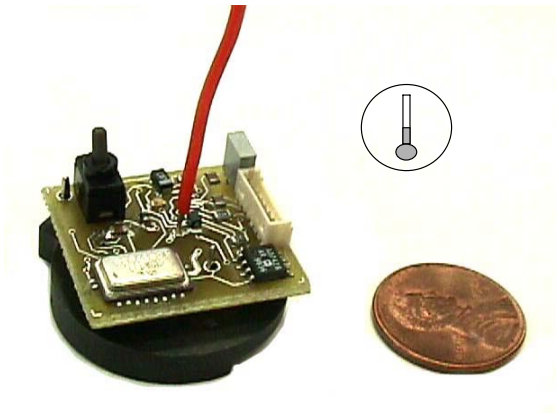

Fig. 35. First Mini RF Mote.

Fig. 36. weC Mote.

3.6 Mote Comparisons

In the previous sections, I discussed the flavors of COTS Dust. In all, there are a total of six functionally different motes: Mouse Collar, CCR Mote, Laser Mote, Steered Agile Beam Mote, RF Mote, and weC Mote. The motes themselves all serve a different function, either in sensor packages or in communication mode. In Table 8 on page 62 the basic mechanical and electrical properties of all the devices are summarized.

Table 8: Mechanical, Electrical, and Price Comparisons of COTS Dust

	dimensions	total part number	price in small quantity	battery capacity @ 3 Volts	sleep/awake current @ 3 Volts
Mouse Collar	0.5”x0.5”x0.3”	12	$25	48 mA-hrs	15uA/1.2mA
CCR Mote	1.1”x1.1”x0.5”	48	$50	560 mA-hrs	50uA/10mA
Laser Mote	1”x1”x2”	50	$91	2550 mA-hrs	1uA/25mA
RF Mote	3”x1”x0.5”	85	$172	1000 mA-hrs	1uA/7mA
weC Mote	1.5” diameter x 0.5”	46	$55	560 mA-hrs	50uA/9.5mA

3.6.1 Computational Power

While COTS Dust devices varied in computational power from 0.03 to 4 MIPS, none of the algorithms I developed exceeded more than 1 MIPS. Table 9 on page 63 shows the algorithms from the demonstrations described in this thesis and the minimum MIPS required to run them. Likewise, program memory was small; none of the programs required more than 2K of memory.

These, of course, are relatively simple examples, and fairly complex distributed sensor algorithms may very well exceed the available memory. While all the algorithms here were written in assembly language, C will likely be the preferred development environment for programmers. C compilers in general do not compact code as well and will result in larger program memories.

Table 9: Code length and computational power for each demonstration

Program	Code Length / total program space	MIPS / total available MIPS
Sensor Retrieval	634/4k	0.15/0.15
Acceleration Sensing	434/4k	0.15/0.15
Laser Weather Station	665/4k	0.01/1.8
Asynchronous CCR demo	1771/4k	0.75/1
Mouse Receiver Collar	~400/768	0.032/0.032

3.6.2 MIPS Efficiency

If energy consumption is a large concern in the design of devices, one would like to have the microprocessor use as little energy as possible. One possible way to reduce power consumption may be to reduce the clock frequency of the microprocessor. However, this does not entirely address the issue. For example, suppose we need to run a pro-

gram on a processor in which the program is one thousand instructions long. At one megahertz the processor finishes its task in 1 ms. Now to save power, we clock the processor at 100 KHz. While the processor consumes less power, it takes 10 times longer to run the same program. Instead of consuming power for 1 ms, the processor consumes power for 10 ms.

An alternative method to examine energy consumption is to look at the total energy required to execute a single instruction, the instruction cost. The instruction cost is measured in Joules/instruction, or for a given voltage MIPS/mA. With this metric, one can choose a processor and speed whose energy is minimized. If we neglect static current in MCU's (see "Static vs. Dynamic Current" on page 11), the dynamic current is equivalent to the instruction cost.

4.0 Design Advice - Failures and Successes

The COTS Dust motes were successfully built and demonstrated. During the design cycle, though, I encountered a number of problems. In this section, I discuss some of the problems I encountered and how I solved them.

I went through two versions of the RF mote before I settled on the one described in this thesis. The first RF mote was designed with a Scenix SX28AC series microprocessor. The SX28AC series can operate with clock cycles up to 50 MHz. However, when I populated my first circuit board, I had trouble getting the RF Monolithics transceiver chipset to work in the presence of the Scenix microprocessor. There are two reasons for why the transceiver chipset did not work correctly. Namely, the receiver was saturated with noise generated by the MCU. The MCU was clocked at a slow speed of 1 MHz, but I believe the fast rise and fall times of the MCU contributed to noise in the receiving band. Secondly, the circuit board did not contain a ground or power plain. Ground and power planes in circuit boards help isolate signals from one another and maintain a stable power supply voltage. The engineers from RF Monolithics recommended a ground plain directly under the receiver on the top circuit board layer with multiple vias connecting it to a global ground plane underneath. In the second version of the RF mote I chose the Atmel AVR microprocessor whose maximum clock speed was no more than 4 MHz. Its low frequency and power operation suggested that the noise generated in the RF band would be lower than that of the Scenix chips. In addition, I added a comprehensive ground plane and physically separated the RFM chipset from the rest of the components on the board.

Another problem in the first version was the choice of power supplies. Because the Scenix MCU operated at 5 volts and the RFM chips operated at 3 volts, I needed a way

to generate both power supplies. My original thought was to use 3 n type alkaline batteries in series to provide 3 and 4.5 volts. Even though the MCU operated at 4.5 volts, the batteries themselves lost voltage over their lifetime. In essence, the batteries voltage dropped from 4.7 volts to 3.9 volts over its lifetime. The voltage quickly fell below the operating range of the MCU. The idea of using two voltage converters for both the MCU and the transceiver chip set was also unappealing due to the added complexity and increased component count. To solve the problem, I focused my designs towards a single operating voltage, namely that of a 3 volt lithium ion battery. All components were designed to operate within the battery range of 2.75 to 3.25 volts.

The circuit boards were designed in Cadence's Orcad Capture and Layout Plus 9.0 tools. I used Techcons System Inc. TS9701 to dispense solder paste. Touch up soldering was done with a Metcal Smartheat soldering iron. Most testing was performed with an HP54645D Digital oscilloscope. Assembly was done by hand, though for large quantities, companies like Quote PCBoards Services, Inc. can also populate the boards.

All code was written in assembly language using Atmel's AVR Assembler 1.30. I recommend, however, writing in C and using a C compiler. Commercial hardware programmers were offered by Atmel. The programmers were so ineffectual that I was forced to design and build my own. Among the problems I encountered with Atmel's programmers were periodic programming failure and driven data lines from the programmer after programming. The homemade programmer was more reliable and did not have any of the draw backs mentioned above. In addition to being a programmer, it also acted as a serial port interface device. With just a few lines of code, one could monitor the behavior of the COTS mote by sending register information over the serial port to the computer. The dual

purpose of the programmer enabled the user to program a device and debug it without changing any of the connections. I cannot emphasize enough the convenience of such a setup.

In the testing of a distributed network, one should pay careful attention to the reprogrammable capabilities of the system. The weC mote is wirelessly programmable, though with limitations. The weC mote uses two MCU's: one MCU runs the normal operations of the device, while the other MCU is used strictly to reprogram the first one. While reprogramming one MCU with the other is possible, considerable software development is required, and in addition, Atmel's AVR MCU's require the whole code to be programmed at one time. Depending on the code length, programming the whole device can take up to 30 seconds. For future devices, I recommend finding a microcontroller that can reprogram its own program memory sections at a time. For example, the Microchip PIC16F877 (see page 10) can reprogram its code one instruction at a time.

The above discussion is not a comprehensive list of the problems I encountered, but it does highlight the most important ones: 1) ground planes, 2) RF noise reduction, 3) single power supply operation, 2) proper programming and debugging utilities, and 4) wireless reprogramming capabilities.

5.0 The Future of COTS Dust

When I refer to COTS Dust I am referring to devices on the order of a cubic inch which contain the four basic subsystems 1) power 2) computation 3) sensors, and 4) communication. Currently, a number of research institutions in the U.S. are working on centimeter-scale distributed sensor networks [26, 27, 28]. While the BWRC group in Berkeley is developing an entire radio on a single CMOS substrate, the WINS group at UCLA is focusing on low power wireless MEMS. Other groups are investigating the routing and connectivity issues that arise from mobile wireless networks [29, 30]. In terms of power, Amirtharajah *et al.* have demonstrated a MEMS system that extracts electric energy from vibrations [31]. Spanos *et al.* have developed wafers with autonomous sensor arrays on them that allow for calibration, control, and monitoring of semiconductor manufacturing processes [32].

The future of COTS Dust communication lies in both RF and optical communication. MEMS is playing an active role in the development of optical micromirrors with integrated lasers [21]. In the near future, complete subsystems in cubic centimeter sizes could be commercialized. A number of impediments, however, stand in the way of the future commercialization of optical communication. To stay competitive with existing RF systems, optical communication systems need to have high data rates. High data rate (~Mbps) imaging receivers are being developed for Smart Dust [18]. In a matter of years, the commercial market could see a low power, high data rate imaging receiver.

Since low power free space optical communication is relatively new, algorithms are still under development to establish optical links between devices. As discussed in “Active Laser Communication” on page 29, establishing optical comm links involves both

spatial and temporal acquisition steps while RF communication only requires temporal acquisition.

RF is a well established field and in the next 10 years will be the communication system of choice for COTS Dust. As mixed signal systems become further integrated onto chips, fully packaged RF transceivers like those from RF Monolithics will become more available. In addition, Bluetooth, a generic communication standard, offers a way for devices to communicate in clusters, much like distributed sensor networks.

Power consumption will also play a key role in the design of COTS Dust. While microcontrollers are following Moore's Law, consuming less power with like functionality, battery energy densities have not improved significantly over the years. Likewise, power consumption of the RF communication systems depends largely on the range of communication. Depending on the application, there will be a direct relationship between battery size and transceiver capabilities.

Since computation will require less power in the future, I expect COTS Dust to migrate to a 32 bit core, for example the Arm core. Even further in the future, custom circuit design could replace commercial microcontrollers as the preferred choice of electronics. Additional functionality would allow future COTS Dust to perform more complex functions: for example, wireless reprogrammability and more intelligent data routing and sensor processing.

6.0 Conclusion

Smart Dust is an ongoing research project whose main goal is to develop cubic millimeter autonomous sensor devices. Because it would take years to develop a single Smart Dust particle, I developed COTS Dust, devices that could be designed and built in one tenth the time yet mimicked the behavior of Smart Dust. COTS Dust provided the testing platform to develop algorithms that could be used in Smart Dust. COTS Dust technology leveraged off the commercial industry. Ready made commercial parts were integrated together to form cubic inch autonomous systems. Like Smart Dust, COTS Dust had four major subsystems: power, computation, sensors, and communication.

In most of the COTS Dust systems, lithium batteries provided the power source. The Atmel AVR microprocessor satisfied the majority of the computation needs of the system. In the literature search, I found that newer microcontrollers offered equivalent power performances with additional functionality. The Atmel 16/32 Strong Thumb for example offers 32 bit processing power with only a fractional increase in power. A number of sensors were also integrated into COTS Dust systems: magnetometers, accelerometers, a light sensor, temperature sensor, pressure sensor, and humidity sensor. By analyzing the data from the accelerometers and magnetometers, the attitude information of the COTS Dust device can be obtained. The Acceleration Sensing Glove (ASG), for example, used the gravity reading off the accelerometers to determine finger orientation of the wearer. The final subsystem of COTS Dust is communication. RF and active and passive laser communication subsystems were successfully built and demonstrated. While RF communication was relatively easy to implement with commercially available products, laser communication demanded that the laser beam be aimed in the exact direction of

the receiving device. Future work could include developing systems which autonomously search and establish communication links via laser beam steering.

With these four subsystems, a number of COTS Dust systems were designed, built, and demonstrated. The earliest member of the COTS Dust family is the RF mouse collar. Enabling biologists to track mice movements in the dark, the collars integrated a very low power microcontroller, RF receiver, and LED. The RF motes integrated the full suite of sensors and demonstrated simple single hop communications protocols. The laser mote established communication over 20 kilometers with less than 3 mWatts of optical power. A MEMS Corner Cube Reflector was integrated into the CCR mote. The CCR mote communicated to an interrogator without having to generate its own laser source. The newest members of the COTS Dust family, the miniature motes, were simplified designs of the RF mote. With a reduced number of sensors and small form factor, the weC mote could be mass produced at a low cost. Currently, Endeavor, a computer science research group at UC Berkeley, is using the weC motes as a vehicle to test their distributed sensor network algorithms.

The appendix at the end of this thesis includes bill of materials and circuit diagrams for the RF Mote, Laser Mote, CCR Mote, and weC Mote. While I am ending my research in COTS Dust, I hope that the information I included in this thesis will provide the foundation for others to develop their own versions of COTS Dust. As long as the commercial industry continues to produce highly integrated chips, COTS Dust can be designed with newer parts and added functionality. Additionally, while I have demonstrated simple algorithms of my COTS Dust systems, I hope Endeavor and related distributed sensor network research can take the algorithm development one step further. Future

work could include designing multi-hop networks, autonomous network configuring, data fusion, and sensor based network decision making. In conclusion, while I have designed, built, and demonstrated the hardware capabilities of COTS Dust, the research is far from being complete. Future work could include both the development of COTS Dust with newer commercial parts and the development of more sophisticated algorithms for distributed sensor networks.

7.0 Bibliography

[1] Stephenson, Neal. *The Diamond Age*, Bantam Books, 1995.

[2] Pister, K.S.J. *http://robotics.eecs.berkeley.edu/~pister/SmartDust/*, March, 2000.

[3] J. M. Kahn, R. H. Katz and K. S. J. Pister, "Mobile Networking for Smart Dust", ACM/IEEE Intl. Conf. on Mobile Computing and Networking (MobiCom 99), Seattle, WA, August 17-19, 1999.

[4] Doherty, L. *Algorithms for Position and Data Recovery in Wireless Sensor Networks*. Master's Report, University of California, Berkeley, June, 2000.

[5] Onset Computer Corporation. *http://www.onsetcomp.com/*, March, 2000.

[6] Arm. *http://www.arm.com/*, March, 2000.

[7] Perng, J. K., Fisher, B., Hollar, S., Pister, K.S.J., "Acceleration Sensing Glove." *ISWC International Symposium on Wearable Computers*, San Francisco, October 18-19th, 1999.

[8] http://www.pumpworld.com/atmos.htm

[9] Crocker, M.J. *Handbook of Acoustics*, John Wiley & Sons, Inc. 1998, pp. 127-128

[10] Ibid. pp. 306-308.

[11] M. Last, K. Pister, "2DOF Actuated Micromirror Designed for Large DC Deflection", MOEMS 99.

[12] Bluetooth. *http://www.bluetooth.com/*, March, 2000.

[13] Jaap Haartsen, Mahmoud Naghshineh, Jon Inouye, Olaf J. Joeresson, and Warren Allen, "Bluetooth: Vision, Goals, and Architecture", ACM Mobile Computing and Communications Review, Volume 2, Number 4, October 1998, pp. 38-45.

[14] RF Monolithics. *http://www.rfm.com/*, March, 2000.

[15] P. B. Chu, N. R. Lo, E. Berg, and K. S. J. Pister, "Optical Communication Using Micro Corner Cube Reflectors", Tenth IEEE International Micro Electro Mechanical Systems Conference (MEMS 97), Nagoya, Japan, Jan. 26-30, 1997, pp. 350-5.

[16] Hsu, Victor S. MEMS corner cube retroreflectors for free-space optical communications: research project. University of California, Berkeley, 1999.

[17] Lambert, Stephen G., Casey, William L. *Laser Communications in Space*, Artech House, Inc. 1995, pp. 97-98.

[18] B. S. Leibowitz, B.E. Boser, K. S. J. Pister, "CMOS "smart pixel" for free-space optical communication", Proceedings of SPIE Vol. 4306 - Sensors and Camera Systems for Scientific, Industrial, and Digital Photography Applications II, San Jose, Jan. 2001.

[19] Nutt, Karen J. (Work in progress) Candidate for Ph.D. in the Department of Integrative Biology at UC Berkeley, June 1998.

[20] J. Hill, R. Szewcyzk, A. Woo, S. Hollar, D. Culler, K. Pister, "System Architecture Directions for Networked Sensors." Proceedings of Ninth International Conference on Architectural Support for Programming Languages and Operating Systems, November 2000.

[21] Matthew Last, *http://www-bsac.EECS.Berkeley.EDU/~mattlast/*, March 2000.

[22] M. Last, S. Patel, B. Fisher, C. Ezekwe, S. Hollar, B. Leibowitz, KSJ Pister, "Video Semaphore Decoding for Free-Space Optical Communication," SPIE Electronic Imaging 2001, San Jose, CA 21-26 Jan 2001.

[23] McLurkin, James. *Algorithms for Distributed Sensor Networks*: research report. University of California, Berkeley, December, 1999.
[24] Endeavour, *http://endeavour.cs.Berkeley.edu/*, March, 2000.
[25] CS294, *http://www.cs.berkeley.edu/~culler/cs294-s00/*, March, 2000.
[26] Berkeley Wireless Research Center, *http://bwrc.eecs.berkeley.edu/*, September, 2000.
[27] Wireless Integrated Sensor Networks, *http://www.janet.ucla.edu/WINS/*, September, 2000.
[28] Mobile Ad-hoc Networks, *http://www.ietf.org/html.charters/manet-charter.html*, September, 2000.
[29] Josh Broch, David A. Maltz, David B. Johnson, Yih-Chun Hu, and Jorjeta Jetcheva, ‘‘A Performance Comparison of Multi-Hop Wireless Ad Hoc Network Routing Protocols.” Proc. of MobiCom ’98, Oct. 1998.
[30] Chalermek Intanagonwiwat, Ramesh Govindan and Deborah Estrin, "Directed Diffusion: A Scalable and Robust Communication Paradigm for Sensor Networks." Proceedings of ACM MobiCom, August 2000.
[31] Rajeevan Amirtharajah, Scott Meringer, Jose Oscar Mur-Miranda, Anantha Chandrakasan, Jeffrey Lang, “A Micropower Programmable DSP Powered using a MEMS-based Vibration-to-Electric Energy Converter,” 2000 IEEE International Solid-State Circuits Conference 2000 Digest of Technical Papers Volume 43, February, 2000, pp. 362-363.
[32] Darin Fisher, Mason Freed, Kameshwar Poolla, C. J. Spanos, “Autonomous Micro-Sensor Arrays for Process Control of Semiconductor Manufacturing Processes,” Proceedings of the 38th Conference on Decision and Control, 1999.

8.0 Appendix A: Bill of Materials

8.1 RF Mote

Part #	Part Value	Part Type	Manufacturer	Distributor	Distributor Part#	Part Description
C1,C25,C10,C11,C12,C1C9,C23,C30,C31	.1 uF			Digikey	PCC104BCT-ND	.1uF Ceramic Capacitor
C6	22 pF			Digikey	PCC220CNCT	22pF ceramic cap 0805 SMD
C24,C28	33 pF			Digikey	PCC330CGCT-ND	33pF 0805 MSD Cap
C7	390 pF			Digikey	PCC391BNCT-ND	390pF ceramic cap 0805 SMD
C20,C21,C27,C29,C32	10 uF			Digikey	PCS1106CT-ND	10uF SM Electrolytic Capacitor
C26	1.0 uF			Digikey	PCS3105CT-ND	1uF SM Tant TE Series
D1				Digikey	P524CT-ND	LED Red Hi Bright
L1,L3				Digikey	PCD1184CT-ND	inductor 1.0uH Fixed SMD
Q3				Digikey	BCX70KCT	Transistor NPN 45V SMD SOT23
Q5,Q6,Q7,Q8,Q9,Q10,Q11				Digikey	NDS352PCT-ND	MOSFET P-CH .5 Ohm SOT23
R14,R22	1 Mohm		Panasonic	Digikey	P1.0MACT-ND	res 1.0M ohm 1/ 10W 0805 SMD
R2,(R12),R39	1.1 kohms		Panasonic	Digikey	P1.1KACT-ND	0805 SMD 5%
R36	1.6 kohms		Panasonic	Digikey	P1.6KACT-ND	0805 SMD 5%
R18	10 kohms		Panasonic	Digikey	P10KACT-ND	0805 SMD 5%
R50,R51,R52	20 kohms		Panasonic	Digikey	P20KACT-ND	0805 SMD 5%
R45,R47,R48,R49	4.7 kohms		Panasonic	Digikey	P4.7KACT-ND	0805 SMD 5%
R38,R37	470 kohms		Panasonic	Digikey	P470KACT-ND	0805 SMD 5%
R33	5.1 kohms		Panasonic	Digikey	P5.1KACT-ND	0805 SMD 5%
R42,R44	5.6 kohms		Panasonic	Digikey	P5.6KACT-ND	0805 SMD 5%
R23	6.8 kohms		Panasonic	Digikey	P6.8KACT-ND	0805 SMD 5%
R35	7.87 kohms		Panasonic	Digikey	P7.87KCCT-ND	0805 SMD 1%
R43,R46	8.2 kohms		Panasonic	Digikey	P8.2KACT-ND	0805 SMD 5%
R40,R41,R53	20 kohm Pot		Bourns	Digikey	TC73X-203ECT-ND	TC73 20kohm trim pot
U4,U42		ADS7841 SSOP	Burr-Brown	Digikey	ADS7841E-ND	IC 12-BIT A/D 4CH serial 16-ssop
U35	5 Connector		Hirose Electric Co.	Digikey	H2202-ND, H2182-ND	5 Connector SM

U51	8 Connector		Hirose Electric Co.	Digikey	H2197-ND, H2185-ND	8 Connector SM
U52	7 Connector		Hirose Electric Co.	Digikey	H2196-ND, H2184-ND	7 Connector SM
U47		LT1635CS8	Linear Technologies	Digikey	LT1635CS8-ND	IC Rail-To-Rail Opamp SO-8
U37,U53,U54		INA2126		Digikey	INA2126U-ND	IC DUAL u-pwr inst amp so-16
U38	5 Kohm	DC95F502W		Digikey	KC002T-ND	Thermistor 5K ohm temp measure
U50		EVQ-PLHA15		Digikey	P8046SCT-ND	momentary switch
X1	32 kHz			Digikey	SE3202-ND	32.768 kHz crystal
X2	149 kHz			Digikey	SE3338	149.475 kHz crystal
U22		ADXL202JQC	Analog Devices	Future Electronics	ADXL202	Accelerometer
U19		SM5310	SMI	SMI	SM5310-015-AH	Pressure Sensor
U24		24LC256-I/SM	Microchip	Bell Industries	24LC256-I/SM	EEPROM
U5		DS1306E	Dallas Semiconductor	Dallas Semiconductor	90-1306E-000	Alarm/Timer
	3V Lithium Battery			Digikey	P126	24MM Lithium w/ PCTERMINAL
U13,U11	Magnetic Sensor	AA002-02	NVE	FLW	AA002-02	NVE 5 ohm resistance bridge tracking
U44		AT90S8515-4AC	Atmel	Insight Electronics	AT90S8515-4AC	MCU
U1		HX2000	RF Monolithics	Spectrum	HX2000	RF 916.5MHz transmitter
U6		RX2010	RF Monolithics	Spectrum	RX2010	RF 916.5MHz receiver
(U21)		IH3605	Micro Switch HyCal	Newark	HIH-3605-B	Humidity Sensor
U28,U29		Antenna	Self made			916.5MHz Antenna
U46				Edmund Scientific	H53371	Silicon Dector 5.1 MM2, p.215 in catalog
(R24)	nothing					

8.2 Laser Mote

Part #	Part Value	Part Type	Manufacturer	Distributor	Distributor Part#	Part Description
C6,C7	12pF			Digikey	PCC120CNCT-ND	
C9,C20	1.0uF			Digikey	PCS3105CT-ND	1uF SM Tant TE Series
C19,C32,C33,C34	0.1uF			Digikey	PCC104BCT-ND	.1uF Ceramic Capacitor
C21	10uF			Digikey	PCS1106CT-ND	10uF SM Electrolytic Capacitor
D1	LED			Digikey	P524CT-ND	LED Red Hi Bright
Q5, Q7	MOSFET P			Digikey	NDS352PCT-ND	MOSFET P-CH .5 Ohm SOT23
Q12,Q13	MOSFET N			Digikey	NDS355NCT-ND	MOSFET N-CH SOT23
R2,R12,R39	1.1K			Digikey	P1.1KACT-ND	0805 SMD 5%
R18	2.2K			Digikey	P2.2KACT-ND	0805 SMD 5%
R35	8.2K			Digikey	P8.2KACT-ND	0805 SMD 5%
R36	1.6K			Digikey	P1.6KACT-ND	0805 SMD 5%
R54,R37	10K			Digikey	P10KACT-ND	0805 SMD 5%
R38	470K			Digikey	P470KACT-ND	0805 SMD 5%
R52	20K			Digikey	P20KACT-ND	0805 SMD 5%
R56,R55	4.7K			Digikey	P4.7KACT-ND	0805 SMD 5%
R57	100 Ohms			Digikey	P100ACT-ND	0805 SMD 5%
R33	5.1K			Digikey	P5.1KACT-ND	0805 SMD 5%
R53	20K Trim Pot			Digikey	TC73X-203ECT-ND	TC73 20kohm trim pot
U5	DS1306	DS1306E	Dallas Semiconductor	Dallas Semiconductor	90-1306E-000	Alarm/Timer
U19	SM5310	SM5310	SMI	SMI	SM5310-015-AH	Pressure Sensor
U21	IH-3605	IH3605	Micro Switch HyCal	Newark	HIH-3605-B	Humidity Sensor
U24	24LC256	24LC256-I/SM	Microchip	Digikey	24LC256-I/SM	EEPROM
U37	INA2126	INA2126		Digikey	INA2126U-ND	IC DUAL u-pwr inst amp so-16
U38	thermistor			Digikey	KC002T-ND	Thermistor 5K ohm temp measure
U46	photodiode			Edmund Scientific	H53371	Silicon Dector 5.1 MM2, p.215 in catalog
U63	Max4331	Max4331				
U51	8connector			Digikey	WM1737-ND, WM1726-ND	8 Connector SM

U52	7connector			Digikey	WM1736-ND, WM1725-ND	7 Connector SM
U53	Laser Connector			Digikey	WM4201-ND, WM2001-ND	
U54,U55	MiniSwitchDPDT	G22AP	NKK			
U56	at90ls8535-4ac			Marshal Industries		
U57	Momentory Switch	GB25A	NKK			
U58	BatteryTerminals			Digikey	WM4200-ND, WM2000-ND	
X1	32.768KHz			Digikey	SE3202-ND	32.768 kHz crystal
X2	1.8MHz			Digikey	CTX067-ND	1.8432MHz Crystal
	Battery Holder					
	Laser		Power Technologies		RS3a670-5	
	Crimp terminal			Digikey	WM2200-ND	crimp, .100
	AAA Batteries					
	Crimp terminal			Digikey	WM1775-ND	1.25 mm crimp
	prototype crimp tool			Digikey	WM9931-ND	

8.3 CCR Mote

Part #	Part Value	Manufacturer	Distributor	Distributor Part #	Part Description
D1	LED	Panasonic-SSG	Digikey	P524CT-ND	LED Red Hi Bright
D2	Schottky Diode	Motorola	Allied Electronics	8582475	Rectifiers by Motorola (MBR0520)
R2	10K		Digikey	P10KACT-ND	0805 SMD 5%
R3	100 Ohms		Digikey	P100ACT-ND	0805 SMD 5%
R4	10K		Digikey	P10KACT-ND	0805 SMD 5%
R5	1.1K		Digikey	P1.1KACT-ND	0805 SMD 5%
R7	75K		Digikey		
R8	30K		Digikey	P10KACT-ND	0805 SMD 5%
R9	16K		Digikey	P10KACT-ND	0805 SMD 5%
R12	51K		Digikey		
R14	11K		Digikey		
R15	51K		Digikey		
R16	1M				
R17	1M				
R18	20K				
R19	91K				
R20	20K				
R21	20K				
R13	trim pot		Digikey		
C1	1.0UF		Digikey	PCS3105CT-ND	1uF SM Tant TE Series
C2	0.1UF		Digikey	PCC104BCT-ND	.1uF Ceramic Capacitor
C3	10UF		Digikey	PCS3106CT-ND	10 UF Electrolyctic Capacitor
C4	100PF		Digikey	PCC104BCT-ND	
C5	100PF		Digikey	PCC104BCT-ND	.1uF Ceramic Capacitor
C6	15UF		Digikey	PCS1156CT-ND	15 UF Electrolyctic Capacitor
C8	0.1UF		Digikey	PCS3105CT-ND	1uF SM Tant TE Series
C9	0.1UF		Digikey	PCS3105CT-ND	1uF SM Tant TE Series
C10	0.1UF		Digikey	PCS3105CT-ND	1uF SM Tant TE Series
C11	100pF				
L1	4.7UH	Sumida	Sumida	CD43-4R7	Inductor 4.7 UH
Q3	NPN				
Q2	PMOS	Fairchild Semi.	Digikey	NDS352PCT-ND	MOSFET P-CH 0.5 Ohm SOT23
Y1	32 KHz crystal	Epson America Inc.	Digikey	SE3202-ND	32.0768 KHz crystal
Y2	0.8 MHz crystal	ECS Inc.	Digikey	X925-ND	800 KHz ceramic resonator
U8	Photodiode	KODAK	Edmund Scientific	H53372	Photodiode detector
U4	AT90LS8535	Atmel	Marshall Industries	AT90LS8535-4AC	Atmel MCU with A/D
U5	AD7418 (Thermistor)	Analog Devices	Avnet		

U7	LT1613 (DC-DC)	Linear Technology	Linear Technoogy		
U10	INA126	Burr Brown			
U9	MAX4334	Maxim			
U12	MAX7414	Maxim			
U11	MAX7413	Maxim			
U6	MiniSwitch DPDT	G23AP	NKK		
U1	Battery Holder	Keystone Elec.	Digikey	1027K-ND	BATTERY HOLDER 23MM DUAL CELL
U13	6Connector	Hirose Electric Co.	Digikey	WM1735-ND, WM1724-ND	7 Connector 1.25 micro miniatur
	Crimp	Waldom / Molex	Digikey	WM1775-ND	Crimp terminal 28-32AWG
	Battery	Panasonic	Digikey	P117-ND	Battery 3V 23mm Lthium Coin type
U2	CCR	BSAC			

8.4 weC Mote

Item	Values	Manufacturer	Distributor	Part Number	Manufac. Number	Description
C1	100pf	Panasonic	Digi-key	PCC101CGCT-ND	ECU-V1H101JCG	100pF 50V Ceramic Cap 0805 SMD
C2,C3	10uF	Panasonic	Digi-key	PCS1106CT-ND		10uF 6.3V Tant TE Series
C4,C10	0.01uF	Panasonic	Digi-key	PCC103BNCT-ND		0.01uF 50V Ceramic CAP 0805 SMD
C5	0.1uf	Panasonic	Digi-key	PCC104BCT-ND	ECU-V1H104KBW	0.1uF 50V Ceramic Chip CAP
C6,C9	13pf	Panasonic	Digi-key	PCC130CQCT-ND		13pF 50V Ceramic 0402 SMD
C7	27pf	Panasonic	Digi-key	PCC270CGCT-ND		27pF 50V Ceramic CAP 0805 SMD
C8	0.015uf	Panasonic	Digi-key	PCC153BGCT-ND	ECU-V1H153KBX	0.015uF 50V Ceramic CAP 0805 SMD
D1	Red LED		Digi-key	L62505CT-ND	CMD17-21VGD/TR8	Hi EFF Red Diff 0805 SMD
D2	Green LED		Digi-key	L62501CT-ND	CMD17-21VRD/TR8	Green Diff 0805 SMD
D3	Yellow LED		Digi-key	L62507CT-ND	CMD17-21VYD/TR8	Yellow Diff 0805 SMD
L1	10nH	Panasonic	Digi-key	PCD1160CT-ND	ELJ-ND10NKF	10nH 10% Fixed SMD
L2	100nH	Panasonic	Digi-key	PCD1172CT-ND	ELJ-NDR10JF	100nH 5% Fixed SMD
L3	Ferrite Bead SMD 0805	Fair-Riate Products	Allied Electronics	2506033017YO		
R1, R9	100 ohms	Panasonic	Digi-key	P100ACT-ND		100ohm 1/10W 5% 0805 SMD
R2	Photo Resistor 100mil		Clairex	CC9PAL		Data Code: 3
R3	270 k	Panasonic	Digi-key	P270KACT-ND		270kohm 1/ 10W 5% 0805 SMD
R4	330 k	Panasonic	Digi-key	P330KACT-ND		330kohm 1/ 10W 5% 0805 SMD
R8, R5	10 k	Panasonic	Digi-key	P10KACT-ND		10kohm 1/10W 5% 0805 SMD
R6	27 k	Panasonic	Digi-key	P27KACT-ND		27kohm 1/10W 5% 0805 SMD
R7	100 k	Panasonic	Digi-key	P100KACT-ND		100kohm 1/ 10W 5% 0805 SMD
R10	8.2 k	Panasonic	Digi-key	P8.2KACT-ND		8.2kohm 1/ 10W 5% 0805 SMD
R11	30 k	Panasonic	Digi-key	P30KACT-ND		30kohm 1/10W 5% 0805 SMD

R12, R13, R14	470	Panasonic	Digi-key	P470ACT-ND	ERJ-6GEYJ471V	470 ohm 1/ 10W 5% 0805 SMD
R17, R15	4.7 k	Panasonic	Digi-key	P4.7KACT-ND		4.7 kohm 1/ 10W 5% 0805 SMD
R16	2.2 k	Panasonic	Digi-key	P2.2KACT-ND		2.2 kohm 1/ 10W 5% 0805 SMD
R18	no part					
U1	TR1000	RFM	Spectrum	TR1000L		916.5 Hybrid ASH Transceiver
U2	at90ls8535-4ac	Atmel	Marshal industries	at90ls8535-4ac		
U3	AD7418AR	Analog Devices	Avnet	AD7418AR		Temperature Sensor
U4	24LC256 I/SM	Microchip Tech Inc.	Digikey	24LC256-I/SM	24LC256-I/ SM	EEPROM
U5	AT90LS2343-4sc	Atmel	Marshal industries	AT90LS2343-4sc		
X1	4MHz		Digi-key	XC587CT-ND	ECS-40-20-18-TR	4.000MHz 20pf SMD
X2	32.768kHz		Digi-key	SE3202-ND	C-002RX 32.768K-A	32.768kHz CYL XTAL C-002 RX Type
J1	12 pin connector		Digi-key	WM1741-ND, WM1730-ND		
SW1	MiniSwitch DPDT		Allied Electronics	870-6043	G22AP	
Crimp		Waldom / Molex	Digikey	WM1775-ND		Crimp terminal 28-32AWG
Battery Holder		Keystone Elec.	Digikey	1027K-ND		BATTERY HOLDER 23MM DUAL CELL
Battery		Panasonic	Digikey	P117-ND		Battery 3V 23mm Lthium Coin type

9.0 Appendix B: Circuit Diagrams

9.1 RF Mote

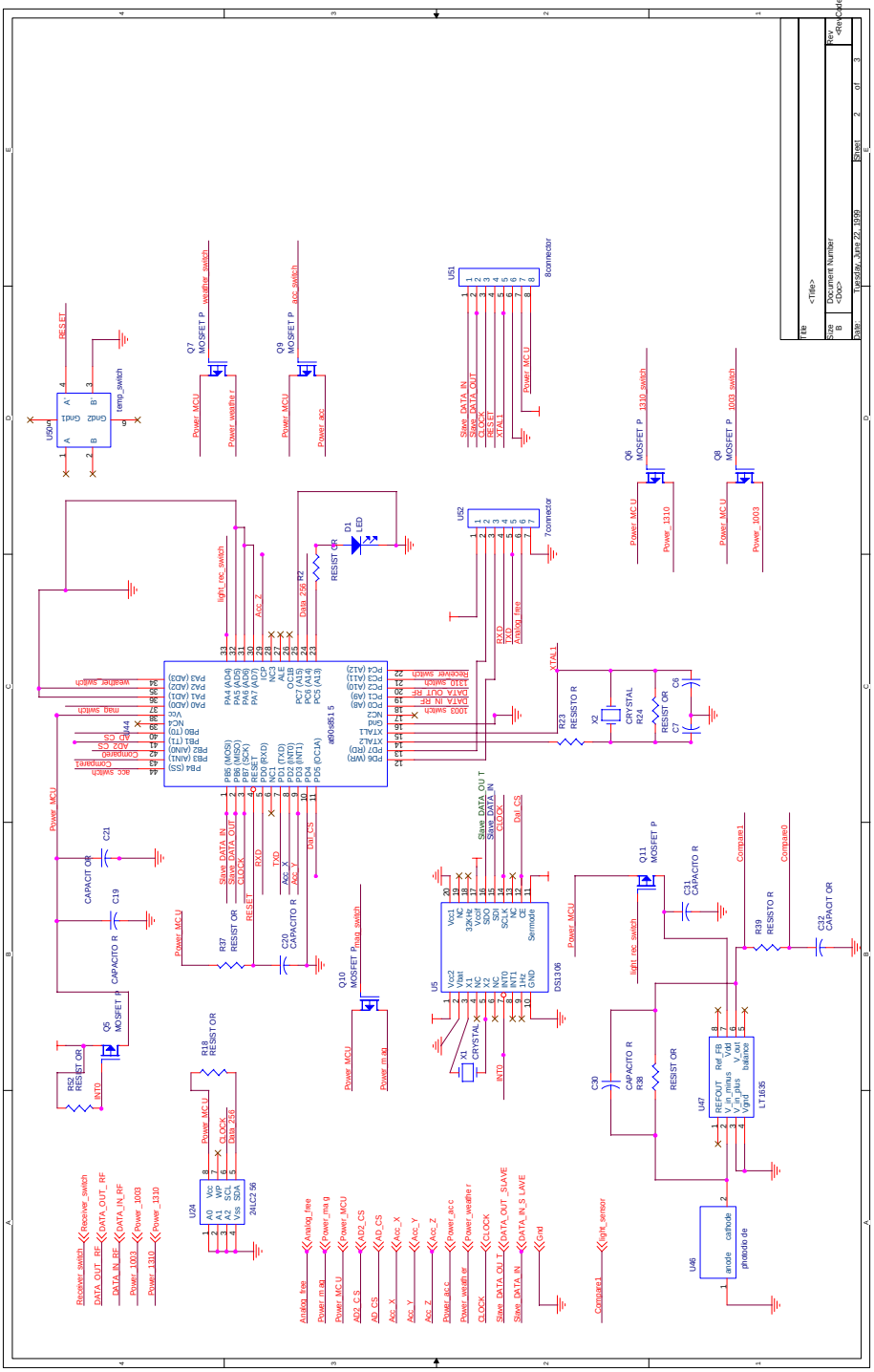

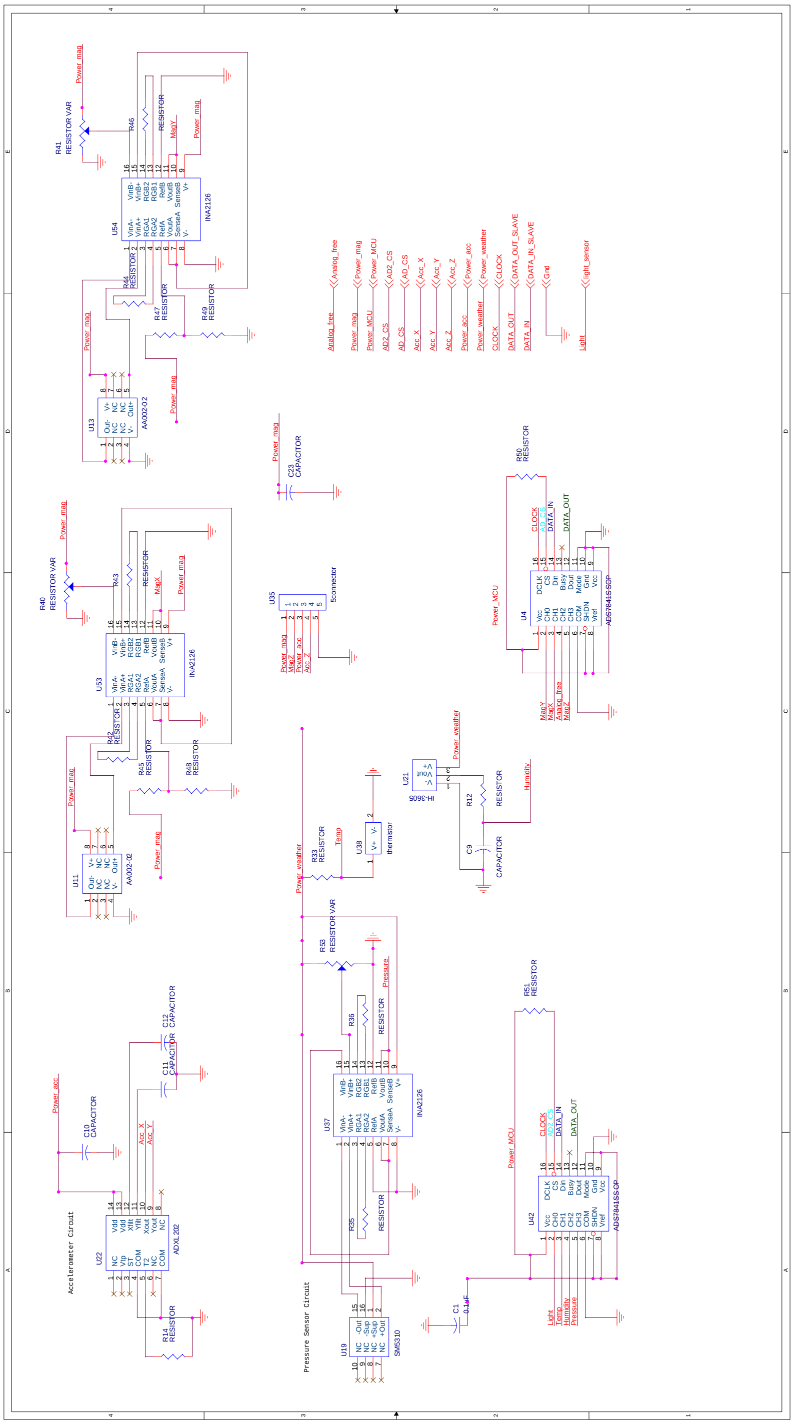
Accelerometer Circuit
Pressure Sensor Circuit
U22
ADXL202
U11
AA002-02
U13
AA002-02
U53
INA2126
U54
INA2126
U37
INA2126
U19
SM5310
U35
5connector
U38
thermistor
U21
IH-3605
U4
ADS7841SSOP
U42
ADS7841SSOP
R40
RESISTOR VAR
R41
RESISTOR VAR
R53
RESISTOR VAR
C10
CAPACITOR
C11
CAPACITOR
C12
CAPACITOR
C23
CAPACITOR
C9
CAPACITOR
C1
0.1uF
Power_acc
Power_mag
Power_MCU
Power_weather
Analog_free
AD2_CS
AD_CS
Acc_X
Acc_Y
Acc_Z
CLOCK
DATA_OUT
DATA_IN
DATA_OUT_SLAVE
DATA_IN_SLAVE
Gnd
Light
light_sensor
Temp
Humidity
Pressure
MagX
MagY

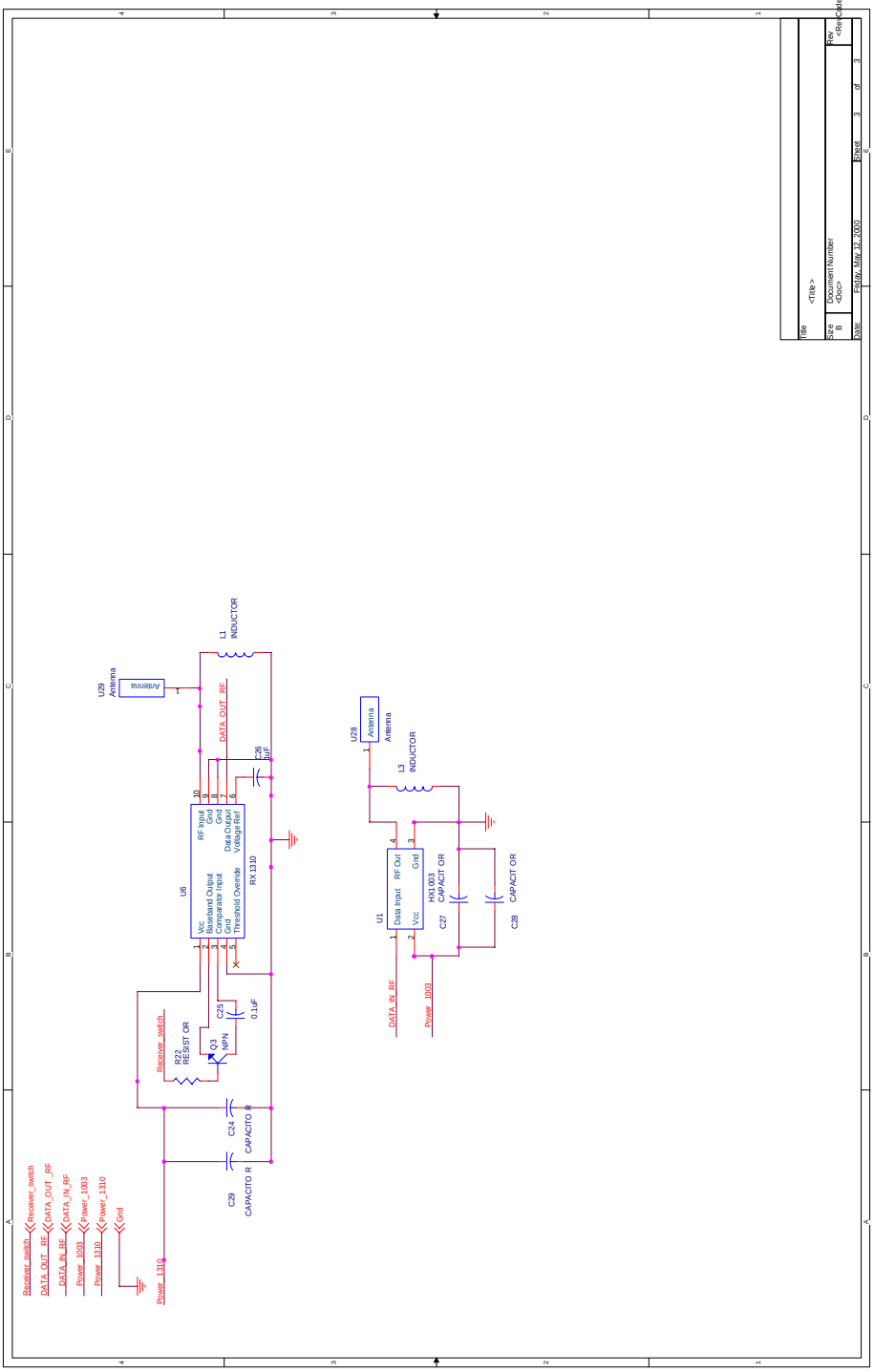
Receiver_switch
DATA_OUT_RF
DATA_IN_RF
Power_1003
Power_1310
Grid
Power_1310
U29
Antenna
antenna
L1
INDUCTOR
DATA_OUT_RF
C26
1uF
U6
Vcc
Baseband Output
Comparator Input
Gnd
Threshold Override
RF Input
Gnd
Gnd
Data Output
Voltage Ref
RX-1310
Receiver_switch
R22
RESIST OR
Q3
NPN
C25
0.1uF
C24
CAPACITO R
C29
CAPACITO R
U28
Antenna
Antenna
L3
INDUCTOR
U1
Data Input
Vcc
RF Out
Gnd
HX1.003
C27
CAPACIT OR
C28
CAPACIT OR
DATA_IN_RF
Power_1003
Title
<Title >
Size
B
Document Number
<Doc>
Rev
<Rev Code>
Date:
Friday, May 12, 2000
Sheet
3
of
3

9.2 Laser Mote

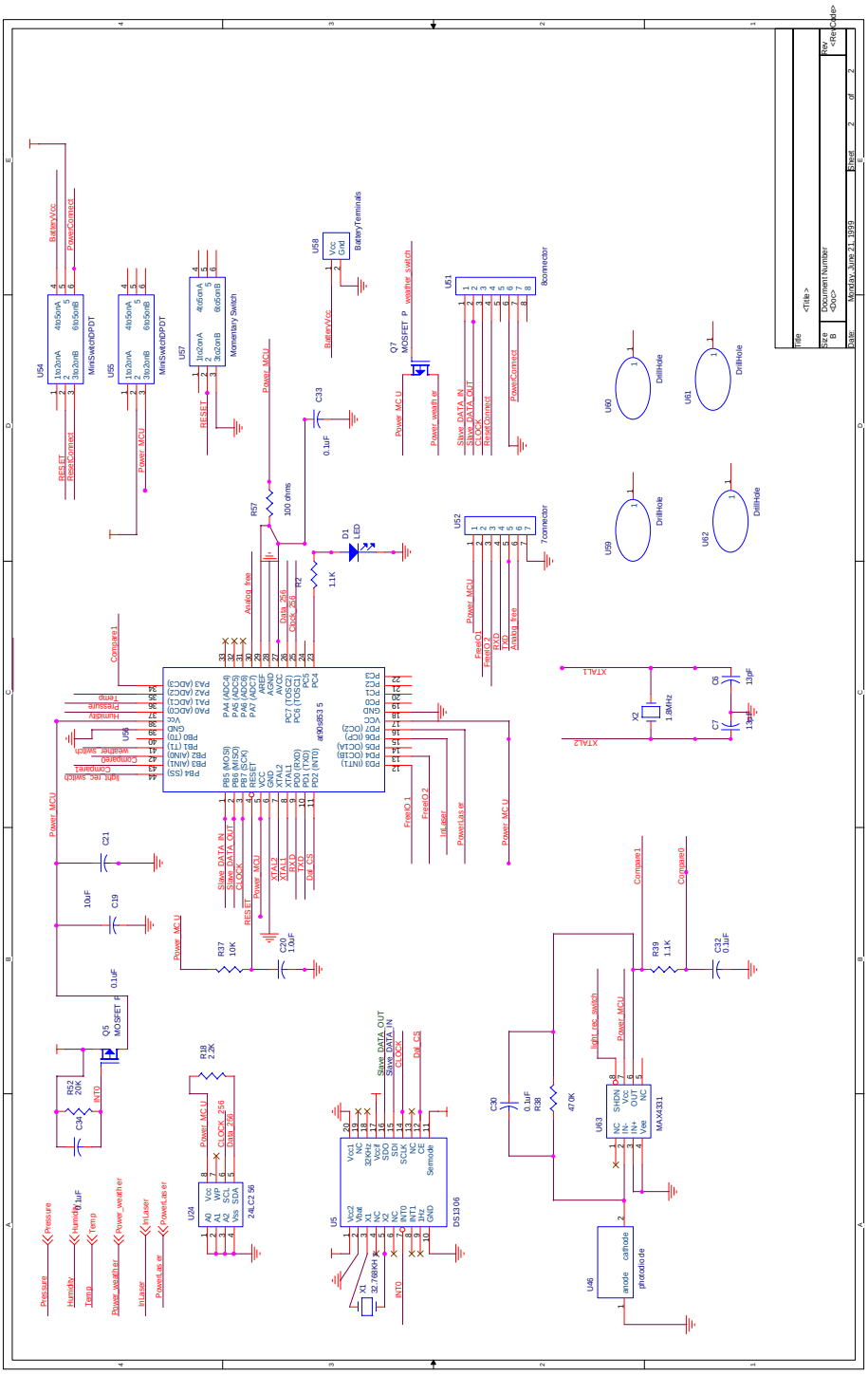

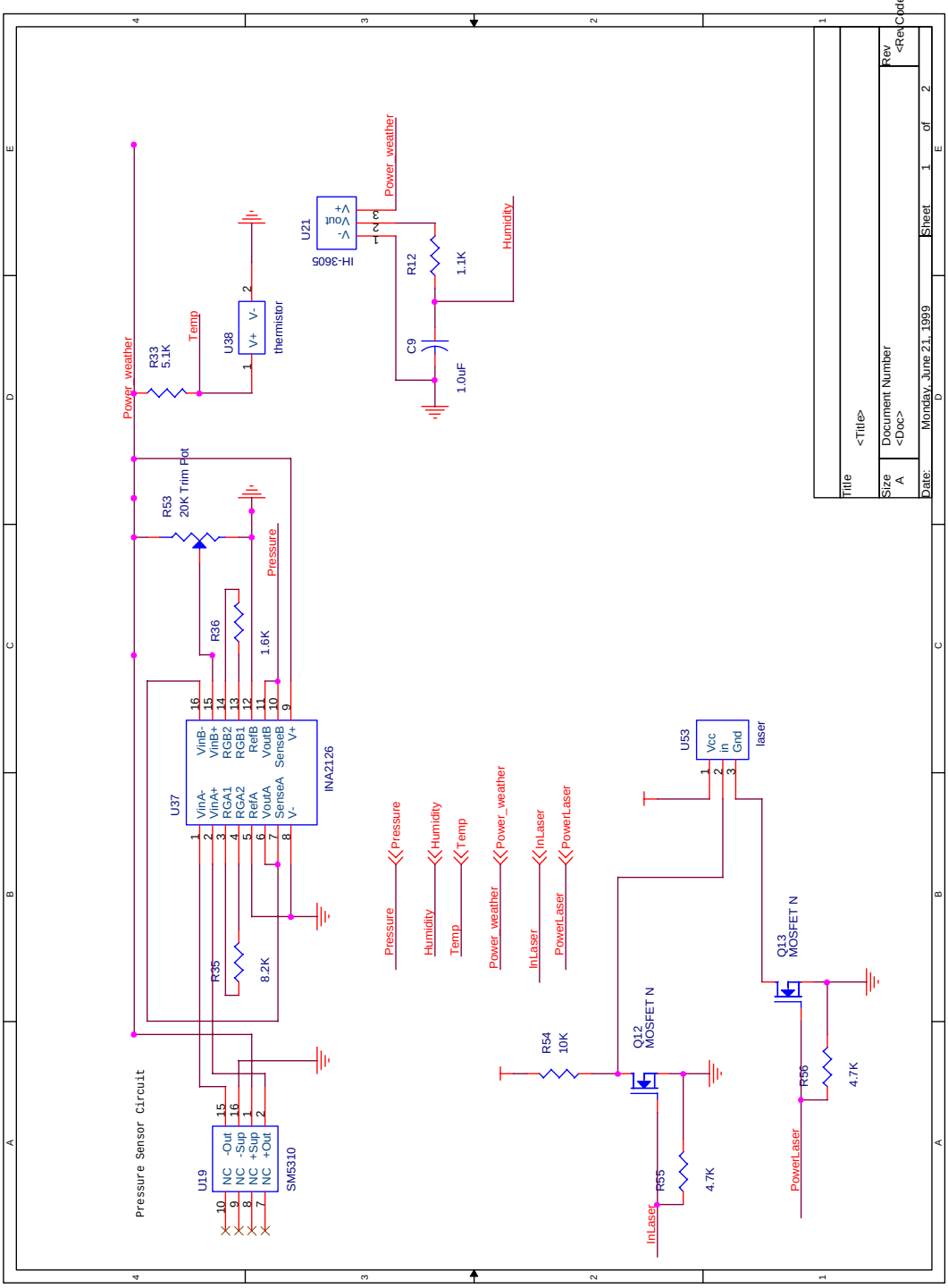
Pressure Sensor Circuit
U19
NC -Out
NC -Sup
NC +Sup
NC +Out
SM5310
U37
VinA-
VinA+
RGA1
RGA2
RefA
VoutA
SenseA
V-
VinB-
VinB+
RGB2
RGB1
RefB
VoutB
SenseB
V+
INA2126
R35
8.2K
R36
1.6K
R53
20K Trim Pot
R33
5.1K
Power_weather
Temp
Pressure
U38
V+
V-
thermistor
U21
IH-3605
Vout
C9
1.0uF
R12
1.1K
Humidity
Pressure
Humidity
Temp
Power_weather
InLaser
PowerLaser
R54
10K
Q12
MOSFET N
R55
4.7K
InLaser
U53
Vcc
in
Gnd
laser
Q13
MOSFET N
R56
4.7K
PowerLaser
Title
<Title>
Size
A
Document Number
<Doc>
Rev
<RevCode>
Date:
Monday, June 21, 1999
Sheet
1
of
2

9.3 CCR Mote

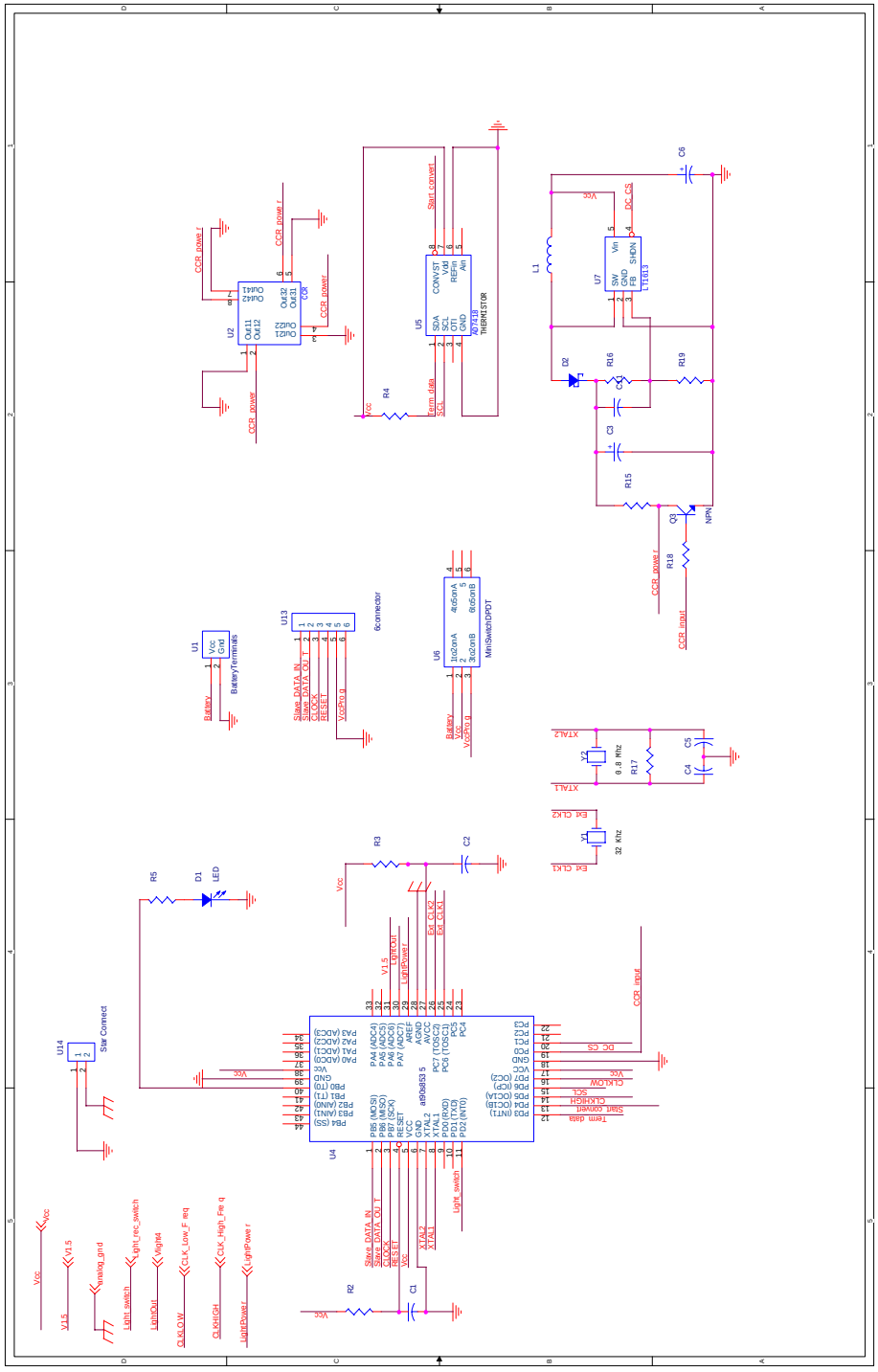

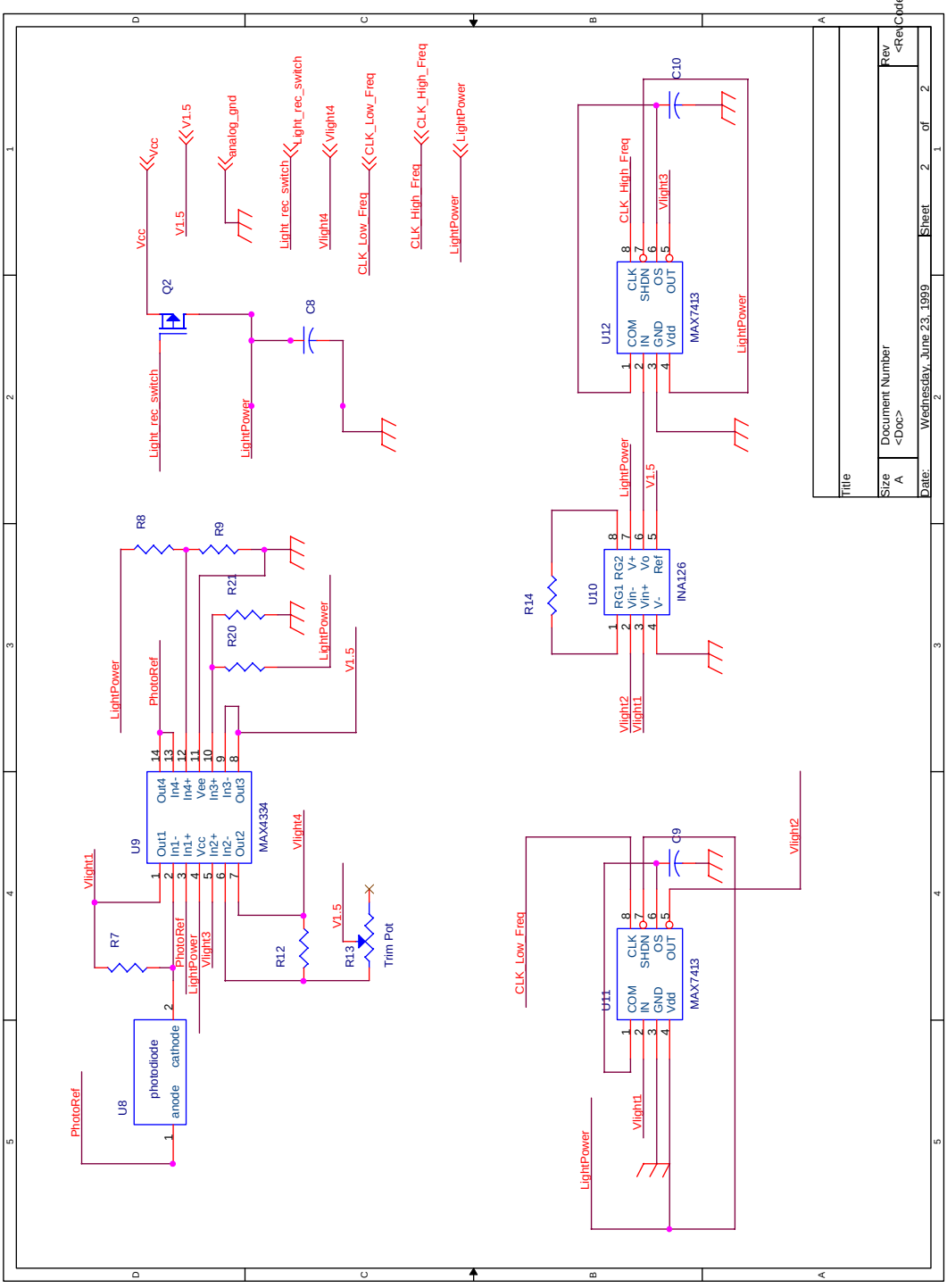
Vcc
V1.5
analog_gnd
Light_rec_switch
Vlight4
CLK_Low_Freq
CLK_High_Freq
LightPower
Q2
C8
R8
R9
R21
R20
R7
R12
R13
Trim Pot
U8
photodiode
anode
cathode
U9
MAX4334
U10
INA126
U11
U12
MAX7413
C9
C10
R14
Vlight1
Vlight2
Vlight3
PhotoRef
Title
Size
A
Document Number
<Doc>
Rev
<RevCode:
Date:
Wednesday, June 23, 1999
Sheet
2
of
2

9.4 weC Mote

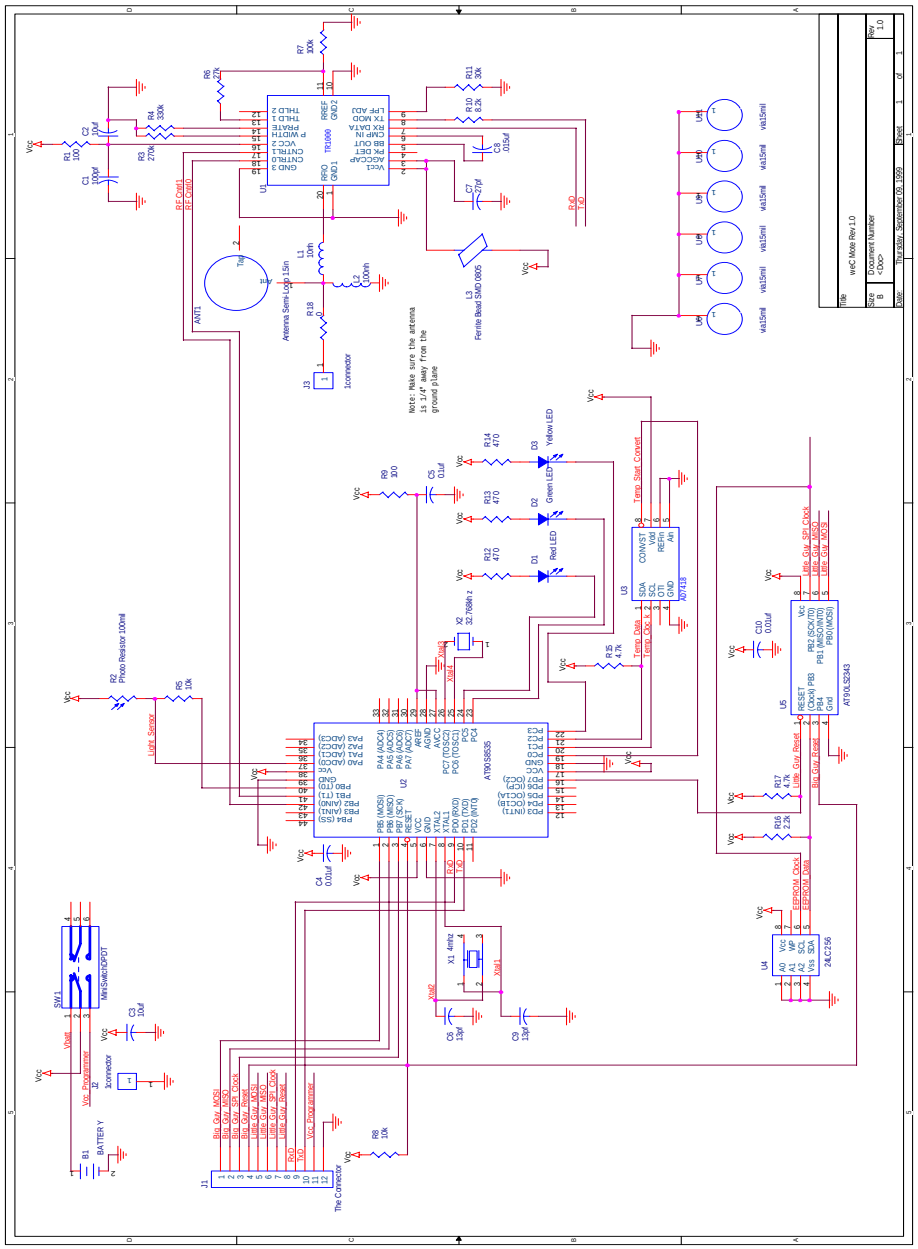
weC Mote Rev 1.0
Thursday, September 09, 1999
Note: Make sure the antenna is 1/4" away from the ground plane
Antenna Semi-Loop 15in
Ferrite Bead SMD 0805
Photo Resistor 100mil
Light Sensor
Red LED
Green LED
Yellow LED
MiniSwitchDPDT
BATTERY
The Connector
Big Guy MOSI
Big Guy MISO
Big Guy SPI Clock
Big Guy Reset
Little Guy MOSI
Little Guy MISO
Little Guy SPI Clock
Little Guy Reset
Vcc Programmer
RFOut1
RFGnd1
Temp Data
Temp Clock
Temp Start Convert
EEPROM Clock
EEPROM Data
ATMEGA8535
AT90LS2343
24LC256
DS1620
TR1000